

Visualizing Entanglement, Measurements and Unitary Operations in multi-Qubit Systems

Jonas Bley,¹ Eva Rexigel,¹ Alda Arias,^{1,2} Nikolas Longen,³ Lars Krupp,^{3,4} Maximilian Kiefer-Emmanouilidis,^{1,3,4} Paul Lukowicz,^{3,4} Anna Donhauser,² Stefan Küchemann,² Jochen Kuhn,² and Artur Widera¹

¹*Department of Physics and Research Center OPTIMAS,
RPTU Kaiserslautern-Landau, 67663 Kaiserslautern, Germany*

²*Faculty of Physics, Chair of Physics Education,
Ludwig-Maximilians-Universität München (LMU Munich), 80539 Munich, Germany*

³*Department of Computer Science, RPTU Kaiserslautern-Landau, 67663 Kaiserslautern, Germany*

⁴*Embedded Intelligence, German Research Centre for Artificial Intelligence, 67663 Kaiserslautern, Germany*
(Dated: May 15, 2023)

In the field of quantum information science and technology, the representation and visualization of quantum states and processes are essential for both research and education. In this context, a focus especially lies on ensembles of few qubits. While powerful representations exist for single-qubit illustrations, such as the infamous Bloch sphere, similar visualizations to intuitively understand quantum correlations or few-body entanglement are scarce. Here, we present the dimensional circle notation as a representation of such ensembles, adapting the so-called circle notation of qubits. The n -particle system is represented in an n -dimensional space, and the mathematical conditions for separability lead to symmetry conditions of the quantum state visualized. This notation promises significant potential for conveying nontrivial quantum properties and processes such as entanglement, measurements and unitary operations in few-qubit systems to a broader audience, and it could enhance understanding of these concepts beyond education as a bridge between intuitive quantum insight and formal mathematical descriptions.

I. INTRODUCTION

Genuine quantum properties are hard to visualize and hence to intuitively understand. Powerful visualizations of simple two-level, single-particle systems such as the Bloch vector representation of the density matrix have been developed to represent properties and dynamics in various situations beyond the mathematical description. Due to the extraordinary mathematical complexity of multi-qubit systems, representing many-body correlations for even two- or few-qubit systems comes along with many challenges.

Geometric representations of pure multi-qubit states and entanglement was previously addressed from the perspective of the mathematical field of topology [1, 2]. Other representations include the Majorana representation depicting multi-qubit states on a Bloch sphere [3] or, alternatively, the use of separate Bloch spheres for the non-entangled part of the system and the entangled part [4, 5]. Also, generalized Wigner functions can be used to represent systems of few qubits [6]. Lastly, a haptic model of entanglement based on knot theory has been proposed [7].

In all of these works, entanglement is geometrically represented. However, they are difficult to generalize to more than two- or three-qubit systems. In addition, the profound mathematical background in, e.g., topology or advanced geometry often needed to understand these models adds multiple layers of complexity. These are, however, often unnecessary in the context of quantum computing algorithms. To solve the latter challenge, various two-qubit visualizations are used for educational purposes [8, 9] and also in the context of

quantum games [10–12].

For more general applications, one needs to go beyond two- or three-qubit systems. Here, graphical languages like the ZX, ZW or ZH calculi, that can be seen as abstractions of circuit diagrams, are commonly used to visualize quantum states and algorithms [13–16]. Their abstractness can be an advantage, e.g., for efficiently showing gate identities and the different possible entanglement properties of multi-qubit system [14]. At the same time, they require an already existing understanding of the often complex underlying concepts and processes. To acquire this understanding, explicit visualizations are necessary.

As such an explicit visualization, the so-called circle notation [17] has been introduced. The aim of this visualization is to minimize the reluctance of learners towards quantum notations and linear algebra formalities, and instead highlight the basic ideas and mechanisms of quantum algorithms explicitly. In this notation, complex numbers are represented graphically by visualizing their magnitude as a filled area in a circle, and their phase as gauge in the circle. A drawback of this visualization is that the action of gate operations on the multi-qubit registers is not intuitive but rather has to be memorized. Furthermore, entanglement remains hidden.

In this work, we present an extension of the circle notation associating every qubit with a separate dimension in space. This new representation visualizes entanglement and provides natural access to quantum operations on multi-qubit registers which enables the explicit visualization of quantum algorithms of up to at least five qubits. We call this extension *dimensional circle notation* (DCN). The approach of assigning qubits to different

dimensions in space is also utilized in [18] for educative purposes, however, considering only real coefficients, thus restricting use cases and prohibiting a general depiction of entanglement that DCN enables. In addition, we show extensions to four- and five-qubit systems.

DCN considers the well known theory of learning and problem solving with multiple external representations (MERs) [19, 20] which aims to support learners' understanding by focusing not only on symbolic-mathematical or text-based representations (e.g., formulas or written text), but also on visual-graphical representations (e.g., pictures and diagrams). In addition, it provides a new perspective on separability of pure multi-qubit states that could be more suitable for learners than the often-used definitions using the density matrix formalism [21–27]. Therefore, we see its relevance as a bridge between single-particle visualization and mathematical many-body descriptions to build intuition for few-body quantum correlations. This can be used, for instance, in courses within the field of quantum information science and technology (QIST) as a facilitator for the construction of conceptual understanding of entanglement and gate operations in multi-qubit systems and, also, beyond education.

This paper is structured as follows: In Sec. II, the underlying theory of MERs and its relevance for the discussion of DCN is described. In Sec. III the circle notation is introduced. It is followed by the introduction of the dimensional circle notation in Sec. IV. Examples in three-qubit systems using DCN are presented in Sec. V. After concluding in Sec. VI, we present an outlook in Sec. VII, where we introduce an interactive DCN web tool and illustrate further extensions of DCN, like visualization of quantum algorithms in four- and five-qubit systems.

II. SUPPORTING CONCEPTUAL UNDERSTANDING IN QIST BY USING MULTIPLE EXTERNAL REPRESENTATIONS

It is well known that learning and problem solving in different contexts of science, technology, engineering, and mathematics (STEM) can be supported by using not only one but multiple external representations (MERs) [20]. In particular, this finding can be utilized in supporting learners' understanding by focusing not only on text-based and symbolic-mathematical representations (e.g., written text and formulas), but also on graphical representations (e.g., pictures and diagrams). From the theoretical perspective, the benefit of using a text accompanied by a graphical representation in learning can be explained by taking advantage of dual coding in the verbal and visual channel of the working memory in contrast to the processing of verbal information only [28, 29]. In this way, information processing is distributed among the two channels, so the load on a channel is lower in comparison when all the information is processed only by single channel.

However, each representation additional to a text implies a new effort for learners, because they need to know how a representation depicts information, i.e., learners need to possess representational competence [30]. Ref. [31] points out that learning with more than two representations, such as a text, an equation and a diagram, is only more efficient than learning with two representations if the learner possesses visual understanding (i.e., representational competence) of each representation. In this line, a representation that encodes complex information in a relatively intuitive way for learners, so that it is easy to acquire representational competence, may be a valuable asset for learning. As mentioned above, up to now, there are only a few representations of multi-qubit systems in QIST and they are rather limited in their capacities, so that it is not easily possible to visualize entanglement and the actions of gate operations. Therefore, DCN enables instructors to encode information in an easily accessible third representation additionally to a descriptive text and mathematical equations to exploit the benefits of MERs for these complex concepts.

Based on Ainsworth's theoretical framework [19], there are three key functions MERs can fulfill to support learning. They can *complement each other* either by containing different information or supporting different processes. Furthermore, they can *constrain each other*, e.g. by familiarity or inherent properties. Third, using MERs can *construct deeper understanding* by confronting learners with the abstraction of underlying knowledge structures, the extension of knowledge to an unknown representation or enhancing understanding of the relations between different representations.

By providing a graphical representation of qubit characteristics and gate operations, we supply learners with additional access to QIST basics complementary to the mathematical notation. In this way, we especially aim to facilitate the understanding of the corresponding mathematical concepts by providing the opportunity to extend existing knowledge structures based on DCN to mathematical formulations. More particularly in the context of entanglement, by using DCN, learners get access to new deciding factors for whether qubit systems or even subsystems are separable or entangled.

However, it is important to note that, in order to benefit from MERs, learners have to cope with understanding of not only how the scientific knowledge is presented in one representation but also how to translate between different representations. Hence, the learning effectiveness of MERs does not only rely on the learning material but also on learner characteristics [19, 32].

In this work, we extend the mathematical formalism of multi-qubit systems and related processes with DCN. Based on current psychological and educational research, we expect that the use of DCN can utilize the known advantages of learning with MERs in QIST by constructing deeper understanding of entanglement and quantum gate operations.

III. CIRCLE NOTATION

We start by briefly introducing the circle notation. In an n -qubit system, there are 2^n different possible basis states represented by 2^n circles. We will work solely in the computational basis as it is commonly used in quantum computing. Here, the basis is given by $\{|i\rangle\}$, $i \in \{0, 1\}^n$, $|i_n i_{n-1} \dots i_1\rangle$, which defines the n -qubit register. Any pure n -qubit state $|\psi\rangle$ can be written as a superposition of these basis states:

$$|\psi\rangle = \alpha_0 |0\dots 0\rangle + \alpha_1 |0\dots 01\rangle + \alpha_2 |0\dots 010\rangle + \dots + \alpha_{2^n-1} |1\dots 1\rangle \quad (1)$$

with $\alpha_i \in \mathbb{C}$, $\sum_{i=0}^{2^n-1} |\alpha_i|^2 = 1$. As per the convention used here, the rightmost entry in the ket state corresponds to the first qubit and the leftmost entry to the n 'th qubit. This means that the least significant qubit in the binary system corresponds to the rightmost entry. As shown in Fig. 1, the circle notation graphically represents the magnitudes of the amplitudes α_i as filled inner circles with radius $|\alpha_i|$ and their phase φ of $\alpha_i = e^{i\varphi}|\alpha_i|$ as the angle between the radial line and a vertical line. Some important single qubit operations (in a single qubit system) are shown in Fig. 13 in Appendix A.

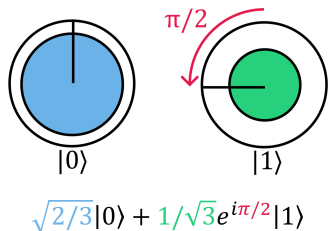


FIG. 1. A qubit in the state $|\psi\rangle = \sqrt{2/3}|0\rangle + 1/\sqrt{3}e^{i\pi/2}|1\rangle$ in circle notation. The outer circles represent the basis states $|0\rangle$ and $|1\rangle$. The radii of the inner circles represent the absolute value of the corresponding coefficients. The radius of the blue circle is $\sqrt{2/3}$ and the radius of the green circle $1/\sqrt{3}$. The blue area is double the size of the green area, showing that measuring would, on average, yield the result 0 twice as often as 1. The angles of the lines in respect to a vertical line represent the phases of the corresponding coefficients. Here, the angle of the line of the coefficient $1/\sqrt{3}e^{i\pi/2}$ of the basis state $|1\rangle$ is horizontal and facing left, representing the phase $\pi/2$.

For two qubits, the possible states are lined up as shown in Fig. 2. In standard circle notation, one can not immediately determine whether the represented state is separable or entangled. We refer to [17] for a precise and comprehensive introduction to the circle notation, in particular, unitary operations and measurements in multi-qubit systems. For calculating their effect, if not memorized, operations require the additional effort of checking each basis state in Dirac ket notation which could reduce the advantage of this representation in respect to

the mathematical representation. We tackle these difficulties with DCN where it is enough to understand these operations in single-qubit systems to understand them in any multi-qubit system.

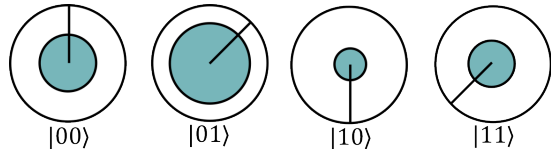


FIG. 2. The two-qubit state $|\psi\rangle = 1/2|00\rangle + 1/\sqrt{2}e^{-i\pi/4}|01\rangle - 1/\sqrt{12}|10\rangle + 1/\sqrt{6}e^{3i\pi/4}|11\rangle$ in circle notation. The states are ordered in ascending order in the binary system, where e.g. the first qubit represents the rightmost number i_1 in a state $|i_2 i_1\rangle$.

IV. DIMENSIONAL CIRCLE NOTATION OF TWO-QUBIT SYSTEMS

Based on circle notation, we introduce DCN as a graphical representation of multi-qubit systems. Instead of arranging states in a row, we assign every qubit to an axis in a new direction in space, see Fig. 3. As shown there, building product states in DCN is an intuitive procedure following the standard Kronecker product. New qubits are simply attached to the original system in a new dimension in space.

a. Separability and Entanglement Entangled states are multi-qubit states that are not separable. In the classical circle notation, see Fig. 2, it is cumbersome to distinguish a separable state from an entangled. In this section, we will show how DCN allows spotting separable states in the two-qubit case. A state $|\psi\rangle = \alpha_{00}|00\rangle + \alpha_{01}|01\rangle + \alpha_{10}|10\rangle + \alpha_{11}|11\rangle$ is separable into $|\psi\rangle = (\alpha_1|0\rangle + \beta_1|1\rangle) \otimes (\alpha_2|0\rangle + \beta_2|1\rangle)$, where \otimes is the Kronecker product, if and only if

$$\alpha_{00}\alpha_{11} = \alpha_{01}\alpha_{10} \quad (2)$$

as stated in, e.g., Ref. [2, p. 396]. We can represent this condition in terms of coefficient ratios $\alpha_{00}/\alpha_{01} = \alpha_{10}/\alpha_{11}$ in the case of $\alpha_{01}, \alpha_{11} \neq 0$ or $\alpha_{10}/\alpha_{00} = \alpha_{11}/\alpha_{01}$ in the case of $\alpha_{10}, \alpha_{11} \neq 0$. In the case of more than two coefficients being 0, the system is trivial. This means we can visually not only identify entangled states, but also get a sense for the degree of entanglement by comparing the ratios of the coefficients $\alpha_{00}/\alpha_{01} = r_1 e^{i\varphi_1}$, $\alpha_{10}/\alpha_{11} = r_2 e^{i\varphi_2}$ in terms of the ratio of their amplitudes r_1/r_2 and the difference of their phases $\varphi_1 - \varphi_2$. For example, the concurrence \mathcal{C} is a common way to measure entanglement [33]. It is defined as $\mathcal{C} = 2|\alpha_{11}\alpha_{00} - \alpha_{10}\alpha_{01}| = 2r_1|1 - r_2/r_1 e^{i\varphi_1 - \varphi_2}|$ for pure two-qubit states (under the assumption of $r_1 > 0$). It can be seen that the concurrence is large for large differences in phases ($|\varphi_2 - \varphi_1| \approx \pi$) and large or small ratios of magnitudes ($r_2/r_1 \gg 1$ or $r_2/r_1 \ll 1$). We compare these ratios for every pair of

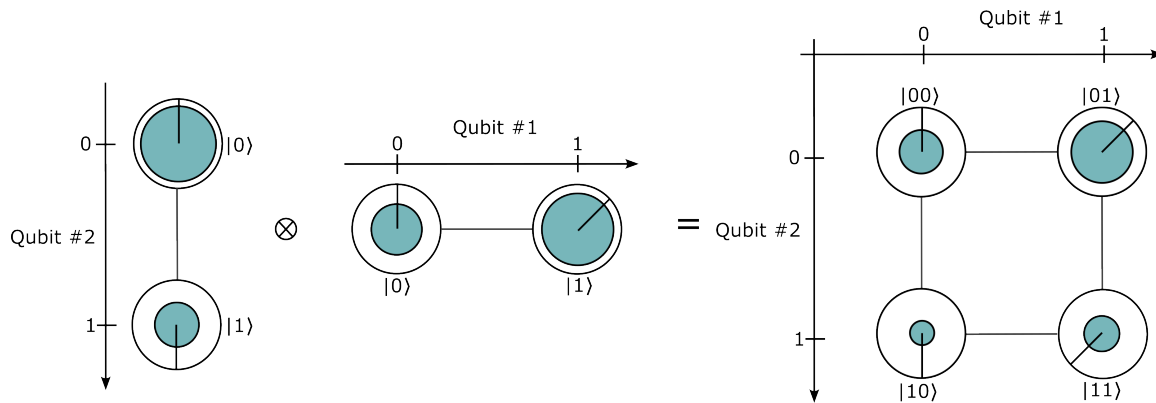


FIG. 3. Visual representation of the product state $|\psi\rangle = (\frac{\sqrt{3}}{2}|0\rangle - \frac{1}{2}|1\rangle) \otimes (\frac{1}{\sqrt{3}}|0\rangle + \frac{\sqrt{2}}{\sqrt{3}}e^{-i\pi/4}|1\rangle) = \frac{1}{2}|00\rangle + \frac{1}{\sqrt{2}}e^{-i\pi/4}|01\rangle - \frac{1}{\sqrt{12}}|10\rangle + \frac{1}{\sqrt{6}}e^{3i\pi/4}|11\rangle$ in DCN. Qubit #1 is attached to each of the basis states of qubit #2 to form a two dimensional array of basis states. The amplitudes of the combined state follow the standard Kronecker product.

states along the axis of one qubit, where both of the corresponding coefficients are non-zero. Then, we can determine whether the system is symmetrical along that axis, apart from a (complex) ratio. If we find symmetry, we know that the system is separable. This is shown in Fig. 4.

It is important to note that this representation of separability into single-particle states only holds if the chosen basis states are themselves separable. We consider exclusively the computational basis here, but in principle any *separable* basis can be used.

b. Measurements Measuring a single qubit, the state collapses into a classical bit of 0 or 1. Similarly, in a terminal measurement of n -qubits the system collapses into the classical bit string $i = i_n i_{n-1} \dots i_1$, where $i \in \{0, 1\}^n$. The measurement of a subset of qubits is, however, more peculiar. In conventional circle notation, see Fig. 2, one needs to precisely identify the subset of qubits measured, by evaluation of the corresponding register state, see [17] for more details. In DCN, we expect this procedure to be more intuitive to understand. A partial measurement (see Fig. 5) in this new dimensional arrangement means that all circles along the measured qubit differing from the measured value turn empty. Afterwards, the state simply has to be renormalized. Furthermore, the probabilities of measuring 0 or 1 are given by the sum of the areas of the inner circles of the basis states corresponding to that value.

c. Unitary Operations Examples of unitary operations in single qubit systems are shown in Fig. 13 in Appendix A. Having understood them and in order to generalize from single-qubit systems to multi-qubit systems in circle notation, one still needs to memorize not only the effects of single qubit operations but instead all possible actions of single qubit gates on all possible qubits. We show here how the dimensional arrangement in DCN eliminates this drawback. Single-qubit gates need only to be applied alongside the axis of the qubit considered. Thus, the visualization of single-qubit operations within

two-qubit systems is transferable from the one-qubit case which importantly still holds for larger qubit systems as we show in the following sections. A comparison of DCN with the standard circle notation is shown in Fig. 6 for the Pauli- X_1 - and X_2 -gates. Note that local unitary operations leave the ratio characterization of separable states intact, i.e., we can not entangle a non-entangled system locally and vice-versa, in agreement with the no-communication theorem [34].

Two-qubit operations also work geometrically in DCN and – again – avoid the necessity of memorizing multiple operations of, e.g., controlled gates where the targeted and controlled qubits are swapped. We show this for two gates that are fundamental to quantum algorithms – the CNOT-gate and the SWAP-gate.

The CNOT-gate applies a NOT (X)-gate to the target qubit if the control qubit has value 1. In DCN, this has a geometrical explanation: the CNOT-gate swaps all states where the control qubit is 1 along the axis of the target qubit as shown in Fig. 7.

The SWAP-gate exchanges two qubits in the system, which is equivalent to swapping the two qubit axes. This gate can be decomposed into three CNOT gates which is relevant in practice because existing quantum computer hardware can often only make use of CNOT gates for qubit interactions. Fig. 8 shows how DCN visualizes this decomposition geometrically.

In Appendix D we provide additional DCN examples for $\text{CNOT}_{12} = (H_2 \otimes H_1)\text{CNOT}_{21}(H_2 \otimes H_1)$ as an example of a phase kickback swapping the role of target and control qubit, see Fig. 14. We also show the Deutsch algorithm which is often considered as an example of quantum parallelism and a (albeit non-practical) use-case of phase kickback, see Fig. 15. The representation of Deutsch algorithm in DCN shows that although a CNOT-gate is present, no entanglement has been created, and therefore the algorithm could, in principle, be realised classically which has been shown in classical optical systems [35].

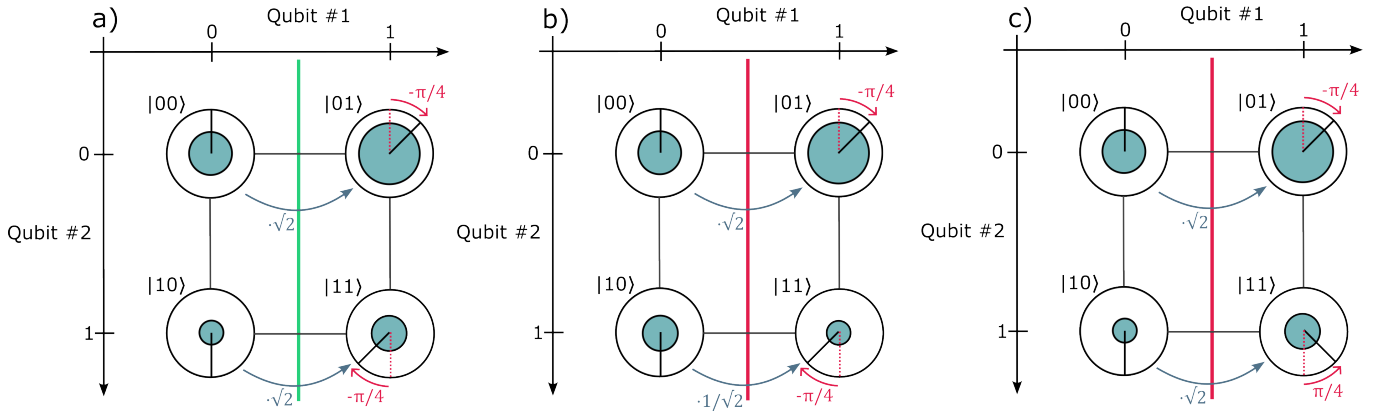


FIG. 4. a) The same two-qubit state as in Fig. 2 and 3, $|\psi\rangle = 1/2|00\rangle + 1/\sqrt{2}e^{-i\pi/4}|01\rangle - 1/\sqrt{12}|10\rangle + 1/\sqrt{6}e^{3i\pi/4}|11\rangle$ and a symmetry axis (green) that shows that this state is separable. The radii of the inner circles are compared in blue gray and the phases are compared in red. The coefficient ratio along this axis is $\alpha_{01}/\alpha_{00} = \alpha_{11}/\alpha_{10} = \sqrt{2}e^{-i\pi/4}$. Along the other symmetry axis, $\alpha_{10}/\alpha_{00} = \alpha_{11}/\alpha_{01} = 1/3e^{i\pi} = -1/3$. b) The state $|\psi\rangle = 1/2|00\rangle + 1/\sqrt{2}e^{-i\pi/4}|01\rangle - 1/\sqrt{6}|10\rangle + 1/\sqrt{12}e^{3i\pi/4}|11\rangle$. It is entangled, because $\alpha_{11}/\alpha_{10} = 1/\sqrt{2}e^{-i\pi/4} \neq \sqrt{2}e^{-i\pi/4} = \alpha_{01}/\alpha_{00}$. c) The state $|\psi\rangle = 1/2|00\rangle + 1/\sqrt{2}e^{-i\pi/4}|01\rangle - 1/\sqrt{12}|10\rangle + 1/\sqrt{6}e^{-3i\pi/4}|11\rangle$. It is (phase-)entangled, because $\alpha_{11}/\alpha_{10} = \sqrt{2}e^{i\pi/4} \neq \sqrt{2}e^{-i\pi/4} = \alpha_{01}/\alpha_{00}$

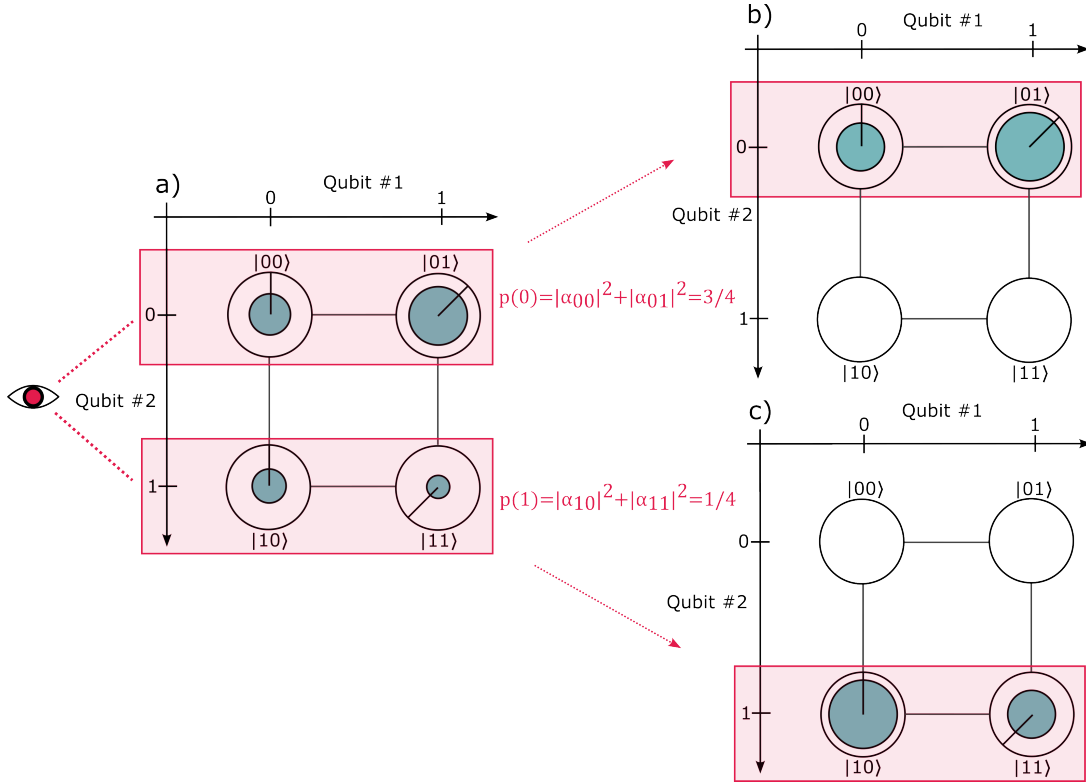


FIG. 5. Measurement of qubit #2 in a two-qubit system in DCN. a) The initial state $|\psi\rangle = 1/2|00\rangle + 1/\sqrt{2}e^{-i\pi/4}|01\rangle + 1/\sqrt{6}|10\rangle + 1/\sqrt{12}e^{3i\pi/4}|11\rangle$ of the system. Comparing the areas of the inner circles, one can see that measuring 0 is more likely than measuring 1. In fact, $p(0) = (1/2)^2 + (1/\sqrt{2})^2 = 3/4$ and $p(1) = 1/4$. b) The state of the system after measuring 0. All circles where qubit #2 is 1 are cleared and the system is renormalized. c) The state of the system after measuring 1.

V. DIMENSIONAL CIRCLE NOTATION IN THREE-QUBIT SYSTEMS

We now shift from two-qubit systems to three-qubit systems and explore the advances of DCN in respect to

standard circle notation. Similarly to the transfer from one-qubit systems to two-qubit systems, DCN operations in three-qubit systems are transferable from the one- or two-qubit cases. Still, the additional qubit leads to a few key differences that we will explain in the following.

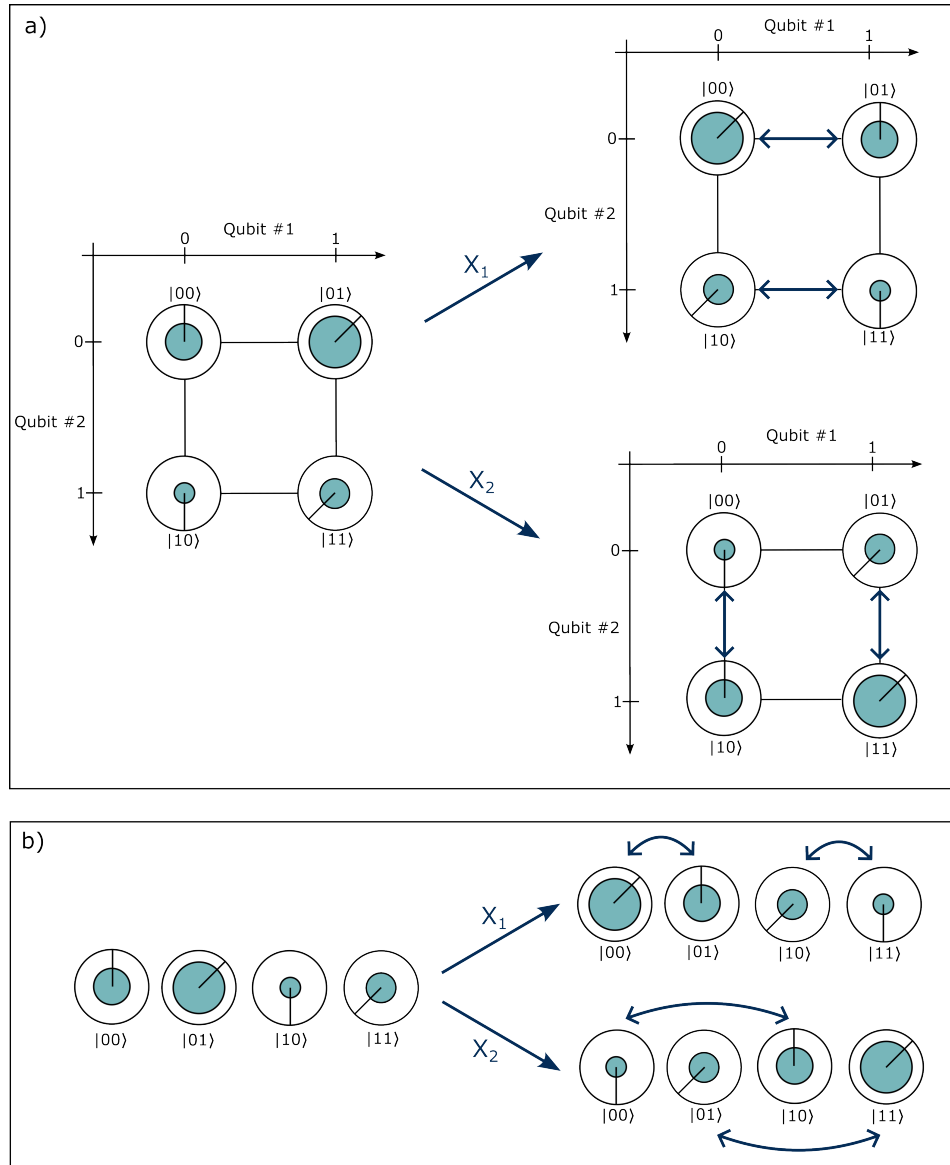


FIG. 6. a) X_1 - and X_2 -gate acting on the two-qubit state $|\psi\rangle = 1/2 |00\rangle + 1/\sqrt{2}e^{-i\pi/4} |01\rangle - 1/\sqrt{12} |10\rangle + 1/\sqrt{6}e^{3i\pi/4} |11\rangle$. The X_1 -gate acts on *all* states along the axis of qubit #1, swapping the coefficients of $|00\rangle$ and $|01\rangle$ as well as the coefficients of $|10\rangle$ and $|11\rangle$. The outcome of the X_1 operation is the state $|\psi\rangle = 1/\sqrt{2}e^{-i\pi/4} |00\rangle + 1/2 |01\rangle + 1/\sqrt{6}e^{3i\pi/4} |10\rangle - 1/\sqrt{12} |11\rangle$. Similarly, the X_2 gate acts on all states along the axis of qubit #2, swapping the coefficients of $|00\rangle$ and $|10\rangle$ as well as $|01\rangle$ and $|11\rangle$. The outcome of the X_2 operation is the state $|\psi\rangle = -1/\sqrt{12} |00\rangle + 1/\sqrt{6}e^{3i\pi/4} |01\rangle + 1/2 |10\rangle + 1/\sqrt{2}e^{-i\pi/4} |11\rangle$. b) The same operations in standard circle notation for comparison.

In addition, we show that DCN is a natural representation for quantum teleportation, which is an algorithm combining many fundamental concepts of QIST like entanglement, unitary operations, and measurement in one protocol.

a. (Partial) Separability and Entanglement To distinguish separable states from entangled ones, we apply a similar procedure taken from the two-qubit case to determine whether a three-qubit system is separable. The two key differences are:

1. In order to compare the ratios of coefficients, we

look for symmetry *planes* instead of axes. This way, we compare the ratios of the top coefficients with the bottom coefficients, left with right or front with back. This is shown in Fig. 9.

2. We have to (and can) differentiate between partial and full separability and compare along two planes. If the ratios are the same along only one plane, we have an entangled two-qubit system that the third qubit, represented by the axis perpendicular to this symmetry plane, is independent of (Fig. 9 is an example of such a state). If and only if the

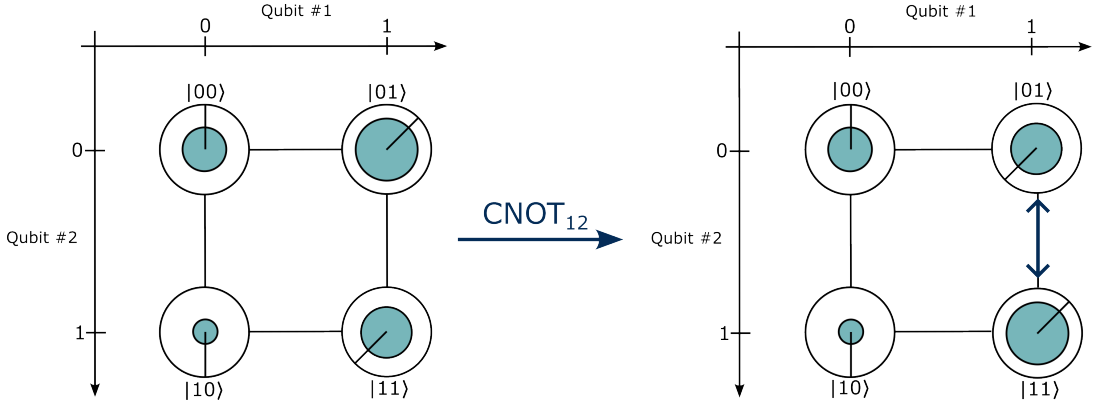


FIG. 7. The two-qubit state $|\psi\rangle = 1/2|00\rangle + 1/\sqrt{2}e^{-i\pi/4}|01\rangle - 1/\sqrt{12}|10\rangle + 1/\sqrt{6}e^{3i\pi/4}|11\rangle$ in DCN and the CNOT_{12} -gate. The CNOT_{12} -gate acts on all states where the control qubit #1 is 1 along the axis of target qubit #2. The outcome of this operation is the state $|\psi\rangle = 1/2|00\rangle + 1/\sqrt{6}e^{3i\pi/4}|01\rangle - 1/\sqrt{12}|10\rangle + 1/\sqrt{2}e^{-i\pi/4}|11\rangle$ represented on the right-hand side. Note that the final state is entangled, as can be seen by comparing the ratio of coefficients along one axis.

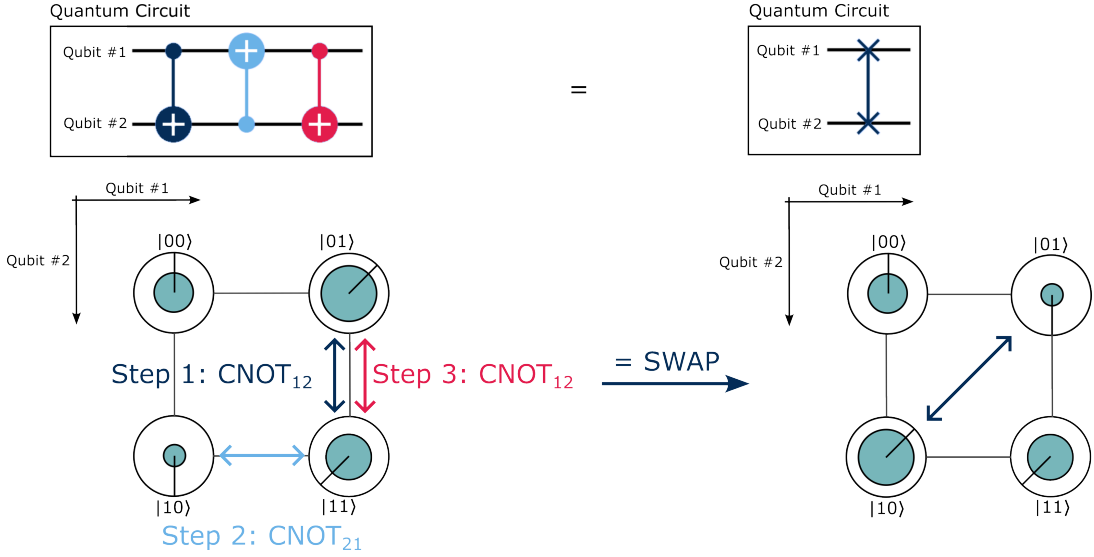


FIG. 8. The SWAP-gate implemented as three CNOT-gates on the two-qubit state $|\psi\rangle = 1/2|00\rangle + 1/\sqrt{2}e^{-i\pi/4}|01\rangle - 1/\sqrt{12}|10\rangle + 1/\sqrt{6}e^{3i\pi/4}|11\rangle$. The corresponding Quantum Circuits are displayed at the top. The relation $\text{CNOT}_{12}\text{CNOT}_{21}\text{CNOT}_{12} = \text{SWAP}$ can be geometrically explained by swapping the states along the two axes step by step. The final state $|\psi\rangle = 1/2|00\rangle + 1/\sqrt{2}e^{-i\pi/4}|01\rangle + 1/\sqrt{6}e^{3i\pi/4}|10\rangle - 1/\sqrt{12}|11\rangle$ is shown on the right hand side.

ratios are the same along two planes, they are also the same along the third plane and we have a fully separable system. This is also stated in more detail in Appendix B and C for the general case of n -qubit systems formulated for the purpose of visualization in DCN [36, 37].

b. Quantum Teleportation Quantum Teleportation has been at the heart of quantum technologies for many years, allowing the transfer of quantum information between two parties over arbitrary distances when an EPR pair is shared between them. It has multiple applications in quantum communication [38] and quantum computation [39, 40] and is therefore an essential part of quantum information processing [41]. Because it incorporates

many fundamental concepts of QIST, quantum teleportation is a suitable example of how DCN could enhance understanding of quantum algorithms in general.

Quantum teleportation works as follows: A pair of entangled qubits #2 and #3 in the state $|\phi^+\rangle_{32} = 1/\sqrt{2}(|00\rangle + |11\rangle)$ is prepared. Qubit #3 is sent to Bob and qubit #2 to Alice. Alice also has qubit #1 in the state $|\psi\rangle_1$ which she does not necessarily need to know and that she wants to teleport to Bob. $|\phi^+\rangle_{32}, |\psi\rangle_1$ and the product state $|\psi\rangle = |\phi^+\rangle_{32} \otimes |\psi\rangle_1$ are shown in Fig. 10 in DCN.

During quantum teleportation, the information of qubit #1 is transferred to qubit #3. Fig. 11 shows that, in DCN, this has geometric meaning: Because of the

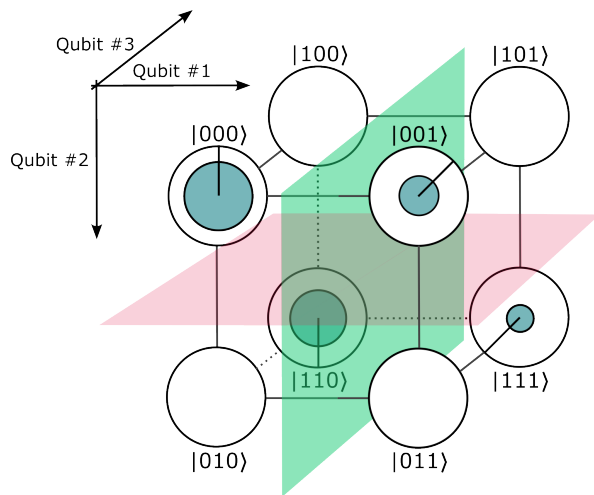


FIG. 9. The partially separable state $|\psi\rangle = 1/\sqrt{2}|000\rangle + 1/\sqrt{6}e^{-i\pi/4}|001\rangle - 1/2|110\rangle + 1/\sqrt{12}e^{3i\pi/4}|111\rangle = (\sqrt{2}/\sqrt{3}|00\rangle - 1/\sqrt{3}|11\rangle) \otimes (\sqrt{3}/2|0\rangle + 1/2e^{-i\pi/4}|1\rangle)$. The green symmetry plane shows that qubit #1 can be separated from the system. However, the system is *not* fully separable because there is no symmetry along the axis of qubit #2, i.e. the red plane is *not* a symmetry plane. Similarly, there is no symmetry along the axis of qubit #3.

equivalence of an axis with a qubit, transferring information from one qubit to another is the same as transferring information from one *axis* to another. This can be done using the unitary operations CNOT_{12} and H_1 . These operations only act on qubit #1 and #2, i.e. along the axis of qubit #1 and #2. In practice, this means that Alice does not need physical access to qubit #3. This transfer of information is only possible due to the entanglement of qubit #2 and qubit #3. To achieve her goal, Alice first applies a CNOT-gate with qubit #1 as control and qubit #2 as target. She then applies a Hadamard-gate to qubit #1. This is shown in Fig. 11.

When Alice now measures qubit #1 and qubit #2, the four possible measurement outcomes 00, 01, 10 and 11 lie on the 2D plane spanned by qubit #1 and qubit #2. The resulting state of qubit #3 depends on the measurement result. Alice sends the result to Bob who applies an X and/or a Z -gate if needed so that his qubit #3 is in the state that qubit #1 previously was in. This is shown in Fig. 12.

VI. CONCLUSIONS

The standard circle notation is already a useful tool for introductory quantum computing courses, as the visualization lowers the barrier to entry into a mathematically challenging field. This is especially needed due to its interdisciplinarity and the various different academical backgrounds of learners [42]. In this paper, we showed that DCN has several advantages over standard circle notation on a conceptual level. This is because DCN vi-

ualizes separability due to the ratio characterization and could make the effect of measurements and unitary operations in two- and three-qubit systems more intuitive due to a geometric depiction of single qubits as parts of these systems.

It is important to consider the conceptual limitations of DCN. First of all, larger than six- to seven-qubit systems will be difficult to visualize due to the exponential scaling of the number of basis states, although one could say that this will be a drawback of any explicit visualization. An important limitation of DCN is that it can not completely replace mathematics for two reasons. Firstly, exact numerical amplitudes and phases are not visible, which, for example, means that many separable states can only *approximately* be identified as such. Secondly, DCN can not display variables and is restricted to specific examples. However, specific examples are often enough and even needed to understand the general case by abstraction.

Lastly, the theory-based educational foundation of DCN lies in Ainsworth's framework of multiple external representations and, more specifically, in the relation and extension of currently used representations to construct a deeper understanding of QIST basics as discussed in Sec. II while complementing the mathematical notation. These theoretical functions of DCN will have to be proven in future systematic empirical education research.

We conclude that DCN can find immediate educational use in introductory quantum computing and quantum technology courses as well as in contexts beyond education to visualize the entanglement properties of and gate operations in multi-qubit systems complementary to the mathematical formalism. It provides a new perspective on entanglement and the geometry of unitary operations in multi-qubit systems and by doing so, it could enhance understanding of quantum algorithms in general.

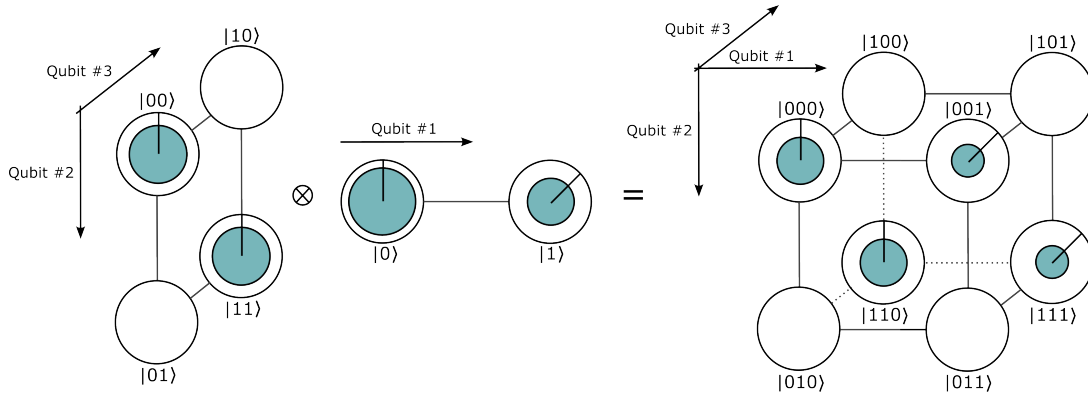


FIG. 10. The initial state in quantum teleportation represented as separate systems and as a three-qubit system. Alice and Bob share the bell pair $|\phi^+\rangle_{32} = 1/\sqrt{2}(|00\rangle + |11\rangle)$ and Alice wants to teleport the state of qubit #1, $|\psi\rangle_1 = \sqrt{2/3}|0\rangle + 1/\sqrt{3}e^{-i\pi/4}|1\rangle$ to qubit #3. The product state $|\psi\rangle = |\phi^+\rangle_{32} \otimes |\psi\rangle_1 = 1/\sqrt{3}|000\rangle + 1/\sqrt{6}e^{-i\pi/4}|001\rangle + 1/\sqrt{3}|110\rangle + 1/\sqrt{6}e^{-i\pi/4}|111\rangle$ is shown on the right hand side.

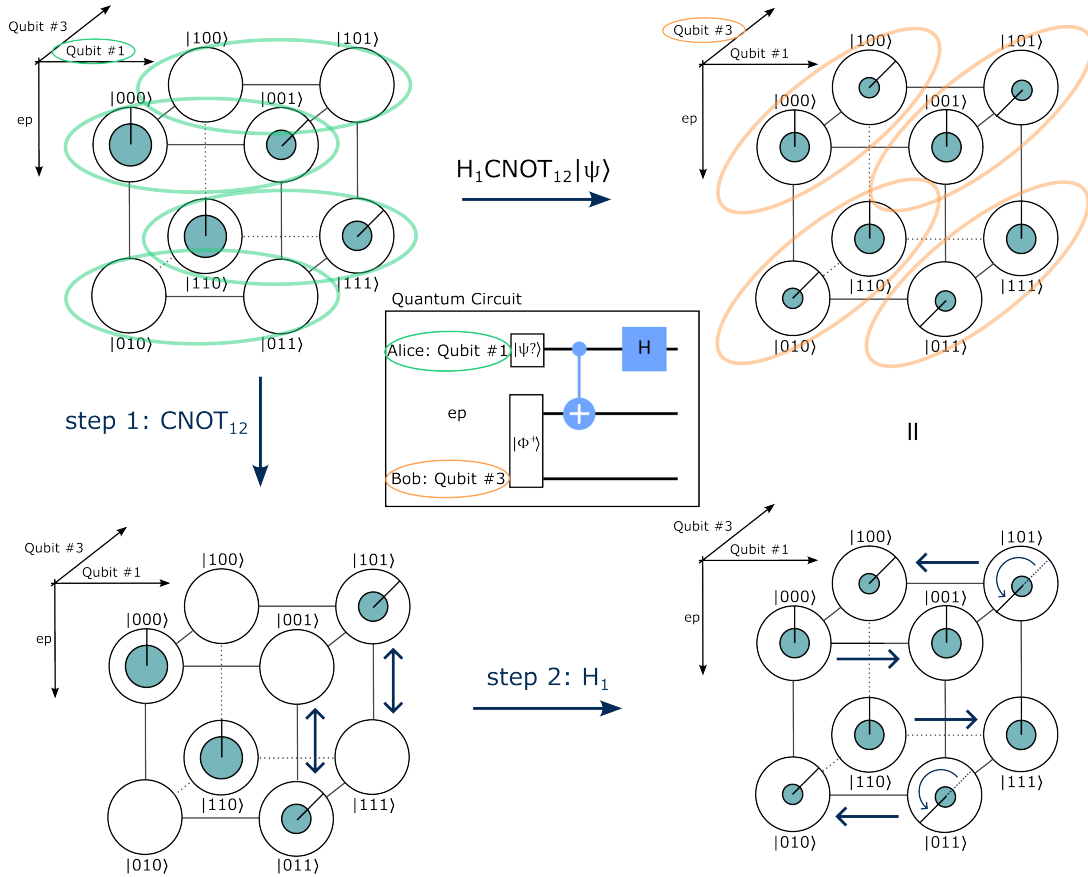


FIG. 11. The central part of the quantum teleportation algorithm. Qubit #1 starts in the arbitrary state $|\psi\rangle_1 = \sqrt{2/3}|0\rangle + 1/\sqrt{3}e^{-i\pi/4}|1\rangle$. Qubits #2 and #3 start in the bell state $|\psi^+\rangle_{32} = 1/\sqrt{2}(|00\rangle + |11\rangle)$. The product state is constructed as shown in Fig. 10. The information that is initially stored in qubit #1 (green) which is independent of the other two qubits is transferred to qubit #3 using only unitary operations on qubit #1 and #2, i.e. operations only along the axes of qubits #1 and #2 in two steps. Step 1: Swap states on the right hand side (where qubit #1 is 1) along the axis of qubit #2 using a CNOT-gate with control qubit #1 and target qubit #2. Step 2: Split states along axis of qubit #1 using a Hadamard-gate on qubit #1. The corresponding quantum circuit is displayed in the top left.

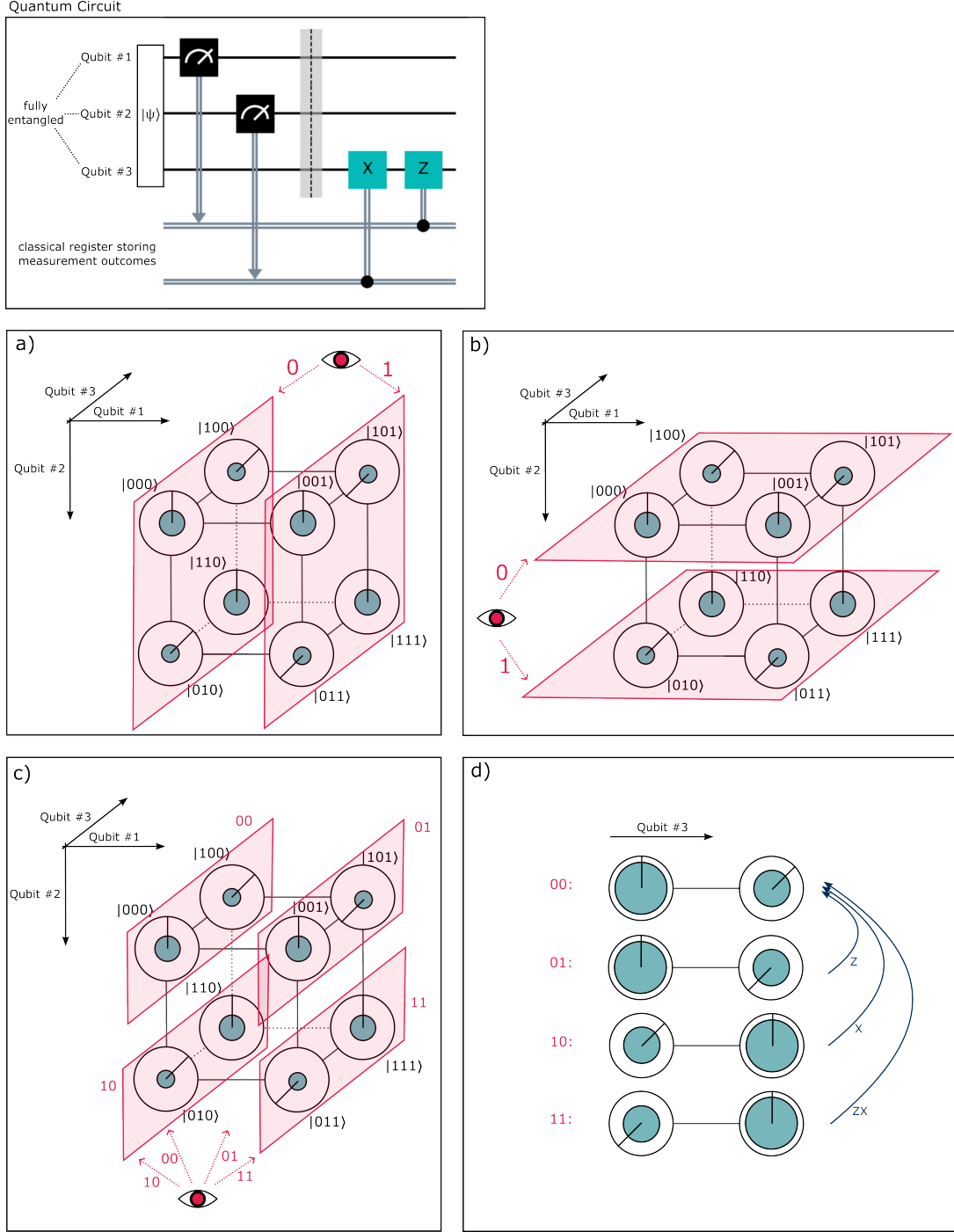


FIG. 12. The last steps of the quantum teleportation process: Alice measures and sends the information to Bob who then applies single-qubit gates according to the measurement result. The corresponding quantum circuit is displayed in the top left. The system starts in the fully entangled state $2|\psi\rangle = (\sqrt{2/3}|0\rangle + 1/\sqrt{3}e^{-i\pi/4}|1\rangle)|00\rangle + (\sqrt{2/3}|0\rangle + 1/\sqrt{3}e^{3i\pi/4}|1\rangle)|01\rangle + (1/\sqrt{3}e^{-i\pi/4}|0\rangle + \sqrt{2/3}|1\rangle)|10\rangle + (1/\sqrt{3}e^{3i\pi/4}|0\rangle + \sqrt{2/3}|1\rangle)|11\rangle$ depicted in Fig. 11. Alice measures qubit #1 and #2 which is shown in DCN. a) The measurement of qubit #1; b) The measurement of qubit #2. c) The combined measurement of qubit #1 and #2. Because the sum of the areas of the inner circles is the same for all of the four possibilities, the chance of measuring any of the four values is 25%. d) The four possible states of qubit #3 depending on the measurement outcome. Bob has to apply an X and/or a Z-gate such that qubit #3 is in the previous state of qubit #1.

VII. OUTLOOK

Following the discussed limitations, we are working on developing an interactive web tool which makes it possible for everyone to visualize quantum operations in DCN. The repositories for this project can be found here: <https://github.com/QuantTUK/>, see also Appendix E, and the website can be accessed via <https://dcn.physik.rptu.de/>.

Furthermore, we show in Appendix F that we can visualize quantum algorithms of up to at least five qubits as is shown there for a four-qubit error detection and a five-qubit error correction algorithm. For this, we "modularize" DCN, arranging qubit systems in a variety of different ways to lay focus on specific entanglement properties and/or the geometry of unitary operations. By doing so, we aim to enhance understanding of complex multi-qubit algorithms.

We can also represent density matrices and partial traces of density matrices in DCN as shown in Appendix G. Here, the ratio characterization of separability applies similarly. This visualization could serve the purpose of making the transition from Dirac ket notation and DCN to the density matrix formalism more intuitive.

Another possible extension is the visualization of qudit-systems (qudits can be in d possible states instead of only two). Gates and algorithms in qudit systems are described in [43]. Although qudits are not in the general focus of quantum computing at the moment, it is possible that they could be relevant at some point as there are some recent advancements [44, 45]. In this context, theorem 3 in [36] can be applied similarly to reveal entanglement properties of such systems.

As pointed out above, it has to be studied whether DCN fosters learning and it needs to be validated as a useful educational tool for conveying the basics of quantum computing. As discussed in Sec. II the effectiveness of DCN likely depends on learner prerequisites. This should be considered in future empirical studies. Even beyond educational contexts, DCN can possibly be used to enhance understanding of many different quantum algorithms in order to shed more light on this complex field. For this, the flexibility of the representation that is shown in Appendix F is a particular strength.

ACKNOWLEDGEMENTS

We thank Stefan Heusler from the WWU Münster for valuable general discussions and specific input regarding basis dependency of qubit models.

M. K-E., P. L. and A. W. acknowledge support by the Quantum Initiative Rhineland-Palatinate (QUIP).

J.B., E.R., A.A., M. K-E., P.L. and A.W. acknowledge support by the project QuantTUK at the RPTU in Kaiserslautern, supported by the Federal Ministry of Education and Research (FKZ13N15995).

N.L., L.K. and P.L. acknowledge support by the project KI4TUK at the RPTU in Kaiserslautern, supported by the Federal Ministry of Education and Research (BMBF) under grant number 16DHBKI058.

A.D., S.K. and J.K. acknowledge support by the project Quantum Lifelong Learning (QL3) at the LMU Munich, supported by the Federal Ministry of Education and Research (BMBF) under grant number 13N16024, and the project DigiQ (EU), supported by the European Union's Digital Europe programme under grant number 101084035.

Appendix A: Single-qubit operations in circle notation

To understand single-qubit operations in multi-qubit systems in DCN, it is enough to understand these operations in single-qubit systems which is one of the main advantages of DCN in comparison to the standard circle notation. Fig. 13 shows some important single-qubit operations in single-qubit systems in circle notation.

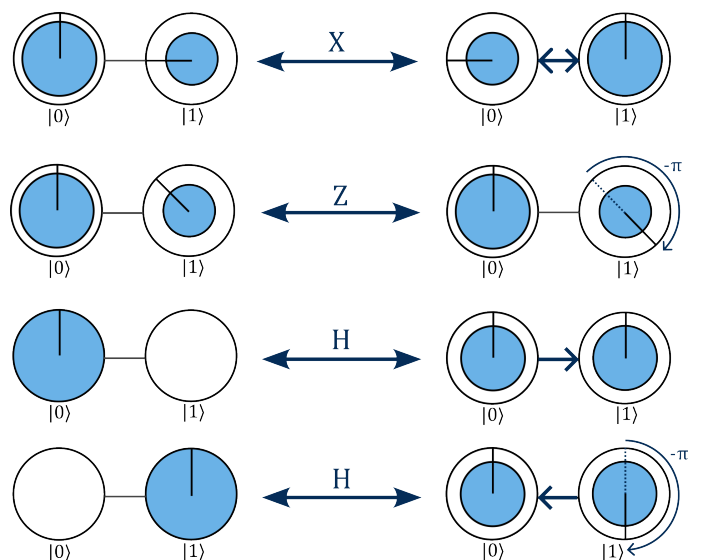


FIG. 13. Single qubit operations in circle notation. The X-gate flips the coefficients of two states. The Z-gate adds a $+\pi$ phase to the $|1\rangle$ -state, flipping the sign of the coefficient. The Hadamard-gate splits a state into two, flipping the phase if starting at $|1\rangle$. All these gates are self-adjoint, i.e. their own inverse.

Appendix B: Separating single Qubits from n -Qubit States

The following ratio characterization [36, 37] of separability in n -qubit systems is used throughout this work to visualize entanglement. It is formulated here for the purpose of showing separability in DCN.

Theorem 1. *Let $\alpha, \beta, c_i \in \mathbb{C}$. An n -qubit state $|\psi\rangle = \sum_{i=0}^{2^n-1} c_i |i\rangle$ is $2 \cdot 2^{n-1}$ separable into $|\psi\rangle = (\alpha |0\rangle + \beta |1\rangle) \otimes \sum_{i=0}^{2^{n-1}-1} c'_i |i\rangle$ if and only if for all $i \in \{0, \dots, 2^{n-1}-1\}$ either $c_{2^{n-1}+i} = 0$ or there exists a ratio $r \in \mathbb{C}$ such that $c_i = r c_{2^{n-1}+i}$.*

Proof. " \Rightarrow ": Let first $|\psi\rangle = \sum_{i=0}^{2^n-1} c_i |i\rangle$ be separable into $|\psi\rangle = (\alpha |0\rangle + \beta |1\rangle) \otimes \sum_{i=0}^{2^{n-1}-1} c'_i |i\rangle$. Then, $|\psi\rangle = \sum_{i=0}^{2^{n-1}-1} \alpha c'_i |0\rangle |i\rangle + \sum_{i=0}^{2^{n-1}-1} \beta c'_i |1\rangle |i\rangle = \sum_{i=0}^{2^{n-1}-1} \alpha c'_i |i\rangle + \sum_{i=2^{n-1}}^{2^n-1} \beta c'_i |i\rangle$. If $\beta = 0$, then $c_{2^{n-1}+i} = \beta c'_i = 0$ for all $i \in \{0, \dots, 2^{n-1}-1\}$. If $\beta \neq 0$, then with $r = \alpha/\beta$: $r c_{2^{n-1}+i} = c_i$, again, for all $i \in \{0, \dots, 2^{n-1}-1\}$.

" \Leftarrow ": Let first $c_{2^{n-1}+i} = 0$ for all $i \in \{0, \dots, 2^{n-1}-1\}$. Then, $|\psi\rangle$ is separable into $|\psi\rangle = |0\rangle \otimes \sum_{i=0}^{2^{n-1}-1} c'_i |i\rangle$. Let otherwise $c_i = r c_{2^{n-1}+i}$. Then, $|\psi\rangle = \sum_{i=0}^{2^{n-1}-1} r c_{2^{n-1}+i} |i\rangle + \sum_{i=2^{n-1}}^{2^n-1} c_i |i\rangle = r |0\rangle \sum_{i=0}^{2^{n-1}-1} c_{2^{n-1}+i} |i\rangle + |1\rangle \sum_{i=0}^{2^{n-1}-1} c_{2^{n-1}+i} |i\rangle = (r |0\rangle + |1\rangle) \otimes \sum_{i=0}^{2^{n-1}-1} c_{2^{n-1}+i} |i\rangle = (\alpha |0\rangle + \beta |1\rangle) \otimes \sum_{i=0}^{2^{n-1}-1} c_{2^{n-1}+i}/\beta |i\rangle = (\alpha |0\rangle + \beta |1\rangle) \otimes \sum_{i=0}^{2^{n-1}-1} c'_i |i\rangle$ with $r = \alpha/\beta$. \square

Appendix C: Full Separability of n -Qubit States

Theorem 1 can be used in fully separable systems for every qubit [37]. Again, here we formulate this for the purpose of showing full separability in DCN.

Theorem 2. *Let $\alpha_i, \beta_i, c_i \in \mathbb{C}$. An n -qubit state $|\psi\rangle = \sum_{i \in \{0,1\}^n} c_i |i\rangle$ is fully separable into $|\psi\rangle = (\alpha_n |0\rangle + \beta_n |1\rangle) \otimes \dots \otimes (\alpha_1 |0\rangle + \beta_1 |1\rangle)$ if and only if for all $j \in 1, \dots, n$:*

for all pairs of bit strings $i, i' \in \{0,1\}^n$ which only differ at position j such that $i_j = 0$ and $i'_j = 1$ and $i_k = i'_k$ for all $k \neq j$:

either $c_{i'} = 0$ (for all such i') or there exists a ratio $r_j \in \mathbb{C}$ such that $c_i = r_j c_{i'}$.

Proof. In the two-qubit case, Theorem 2 is the same as Theorem 1. Assume that Theorem 2 is correct for $n-1$ qubits and let $|\psi\rangle = \sum_{i \in \{0,1\}^n} c_i |i\rangle$. Let, without loss of generality, $j = n$. Then, according to Theorem 1, $|\psi\rangle$ is separable into $|\psi\rangle = (\alpha_n |0\rangle + \beta_n |1\rangle) \otimes \sum_{i=0}^{2^{n-1}-1} c'_i |i\rangle = (\alpha_n |0\rangle + \beta_n |1\rangle) \otimes |\psi'\rangle$ if and only if for all $i, i' \in \{0,1\}^n$ with $i_n = 0$ and $i'_n = 1$ and $i_k = i'_k$ for all $k \neq n$: either $c_{i'} = 0$ for all i' , or there exists a ratio $r_n \in \mathbb{C}$ such that $c_i = r_n c_{i'}$. Then, we can apply Theorem 2 to the $n-1$ -qubit state $|\psi'\rangle$. \square

Appendix D: Multi-Qubit Gates and Algorithms in two-Qubit Systems

Phase kickback is an inherently quantum concept and an essential part of quantum computing. The main idea

is that by local basis transformation, operations with a control and a target qubit are inverted such that the roles of control and target qubit are swapped. This happens because the control qubit inherits the phase of the target qubit while the target qubit is unchanged. This has applications in, e.g., so-called oracle functions that are part of many quantum algorithms – the controlled gates are applied to a set of auxiliary qubits in the Hadamard basis, such that the logical qubits are changed [46]. Fig. 14 shows the most basic example of a phase kickback and Fig. 15 shows a use case of this: the Deutsch algorithm.

Appendix E: Interactive (web-based) DCN-tool

We provide a python package to visualize DCN, which can be accessed at github.com/QuantTUK/QC-Education-Package. Using this package we built a set of hands-on examples for exploring DCN. For easy and fast access we also provide an interactive web tool which utilizes the addressed python packages. This web tool can be accessed via <https://dcn.physik.rptu.de/>, the source files are provided at (github.com/QuantTUK/DCN_Webtool). We plan to further extend and improve the package and web tool in the near future, e.g. with visualizations for more than three qubits as discussed in Appendix F.

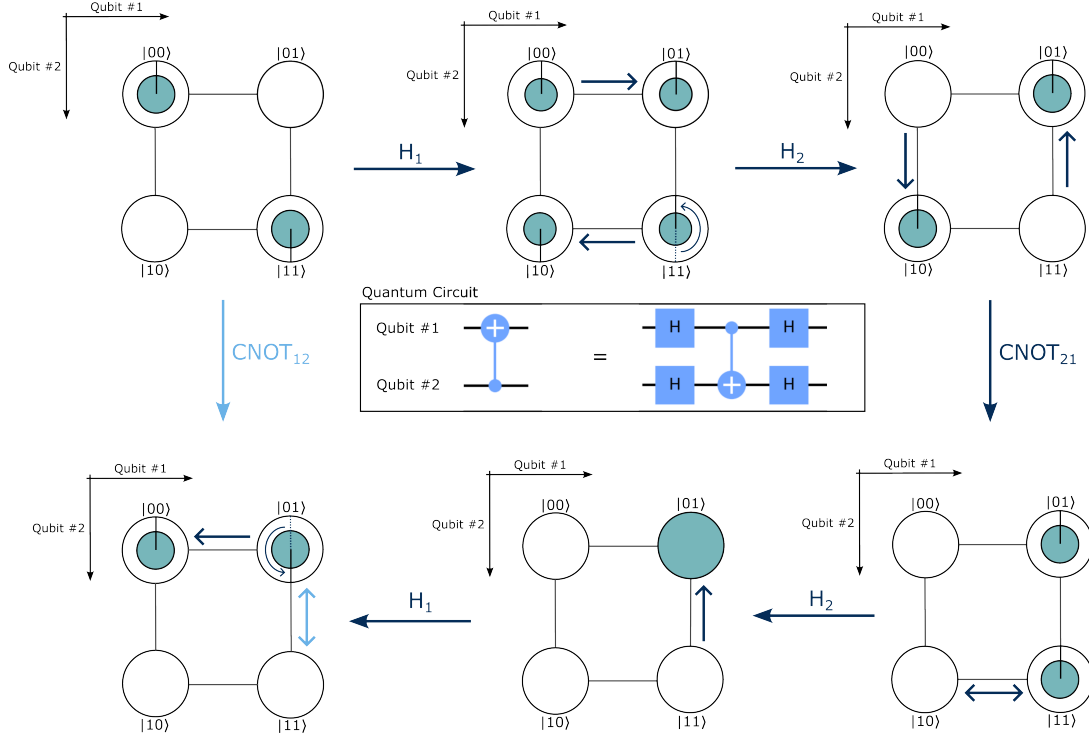


FIG. 14. Basic phase kickback, i.e. the relation $CNOT_{12} = (H_2 \otimes H_1)CNOT_{21}(H_2 \otimes H_1)$, shown with the initial state $|\psi\rangle = 1/\sqrt{2}(|00\rangle - |11\rangle)$. The change of basis into the Hadamard basis by applying Hadamard gates on all qubits makes the $CNOT_{21}$ -gate work like a $CNOT_{12}$ -gate

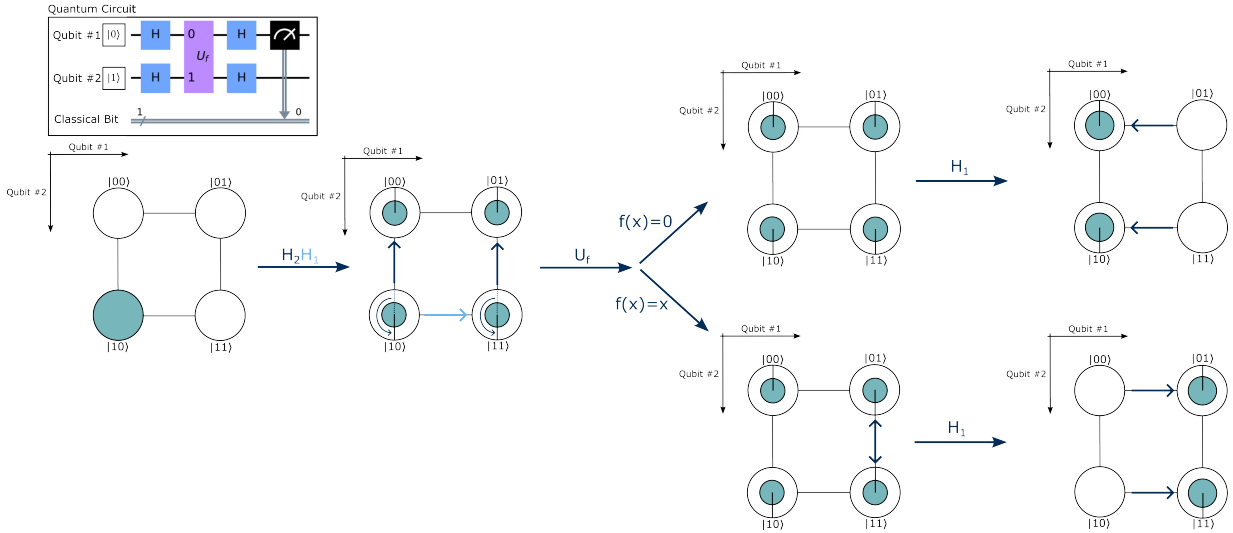


FIG. 15. The Deutsch algorithm to determine whether a function $f : \{0, 1\} \rightarrow \{0, 1\}$ is constant ($f = 0$ or $f = 1$) or balanced ($f(x) = x$ or $f(x) = x \oplus 1$ where $1 \oplus 1 = 0$). The Qubits are initialized to the state $|10\rangle$. After application of Hadamard-Gates on all qubits, the system is in equal superposition with a phase shift on qubit #2. Then the oracle U_f defined by $U_f : |x\rangle|y\rangle \rightarrow |x\rangle|f(x) \oplus y\rangle$ is applied. The two cases where f is constant and the two cases where f is balanced only differ by a global phase, respectively. Therefore, only the cases $f = 0$ and $f(x) = x$ are shown. After application of a Hadamard-Gate on qubit #1, one can see that the operation U_f actually acted on qubit #1 due to phase kickback. When measuring qubit #1, the result will be 0 when f was balanced and 1 when f was constant.

Appendix F: Modular DCN in four- and five-qubit systems

In this section, we give examples on how to represent qubit ensembles of four and five qubits in various ways. There are multiple ways to represent four-qubit systems (systems with 16 basis states) in three dimensional space (and, on paper, then in two dimensions). One natural possibility is a projection of a four dimensional hypercube into three dimensions. This retains the geometric depiction of entanglement that is presented in this paper. For the ratio characterization of separability, eight pairs of coefficients have to be compared for each qubit in order to check for separability of that qubit from the system.

In quantum settings, decoherence is a common factor to consider. Quantum Error correction can counteract the effects of decoherence. Classical error correction is often thought of in terms of hypercubes [47–49]. In fact, similar ideas exist for quantum error correction as seen in hypercubes or hypercube-like lattices [50, 51]. Therefore, it makes sense to apply DCN to quantum error detection and correction. Here, we show the four-qubit error detection code demonstrated experimentally in [52] in Fig. 16 in a hypercube. Note that for a code to also *correct* the detected error, it needs five qubits to function [53].

Another possibility is to represent the system using a mixture of circle notation and DCN that we call modular DCN. We can have two or more qubits on every axis and assign only specific qubits to their own axis. We can then check, again via ratio characterization, separability from the system of the qubits that have their own axis. The five qubit error correction code that is shown in e.g. [54] is visualized in Fig. 17 (simple three-qubit encoding process and three possible single-qubit flip errors), Fig. 18 (transfer Syndrome and error correction in modular $2 \times 2 \times 8$ DCN) and Fig. 19 (the last step of error correction in a four-cube system). DCN is flexible as we can arrange qubit ensembles in modular DCN in a variety of different ways to lay focus on specific multi-partite entanglement properties and/or in a way such that the visualized unitary operations remain geometrically intuitive with the aim of enhancing understanding of complex multi-qubit algorithms.

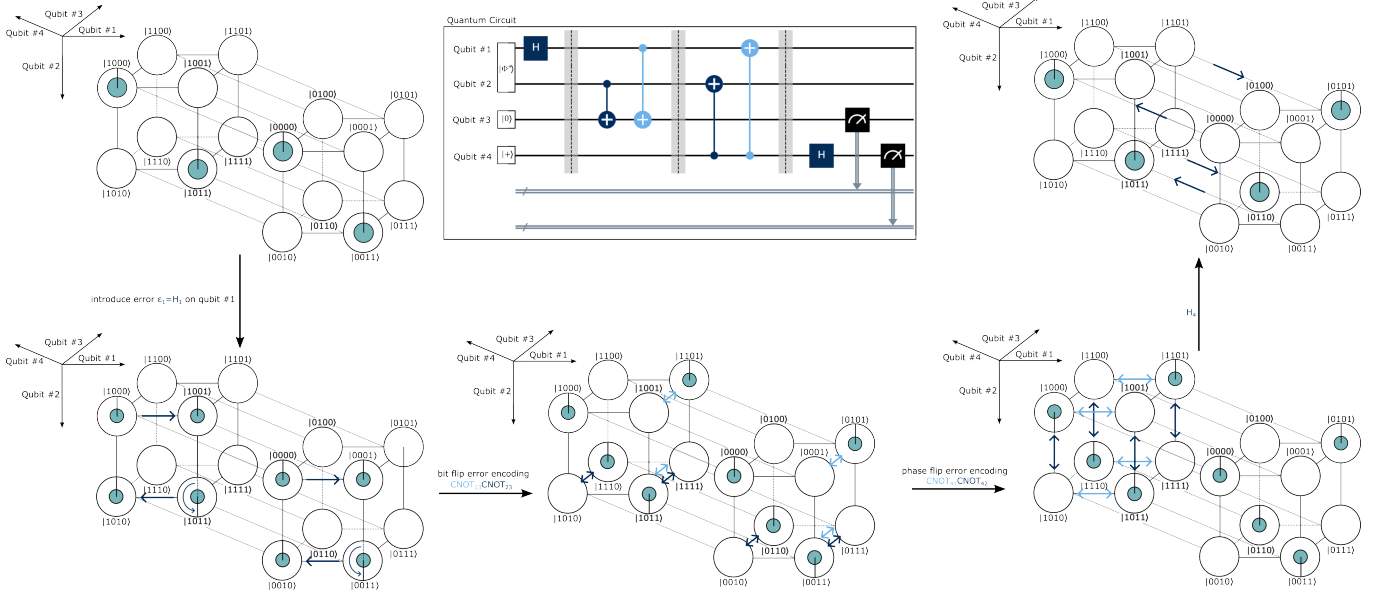


FIG. 16. Four-qubit quantum error detection code as demonstrated experimentally in [52], here in the case of a Hadamard error. The system is initialized to the state $|\psi\rangle = 1/\sqrt{2}(|0\rangle + |1\rangle) \otimes |0\rangle \otimes 1/\sqrt{2}(|00\rangle + |11\rangle)$ where qubit #1 and #2 are entangled and qubit #4 is brought into the Hadamard basis $|+\rangle = 1/\sqrt{2}(|0\rangle + |1\rangle)$ in order to detect a phase flip. First, an error ϵ_1 is applied, in this case a Hadamard error H_1 corresponding to half of a bit flip and half a phase flip on qubit #1. Then, the bit flip error is encoded onto qubit #3 via the $\text{CNOT}_{13}\text{CNOT}_{23}$ operation. Afterwards, the operation $\text{CNOT}_{41}\text{CNOT}_{42}$ that can be seen as a 180° rotation of the cube corresponding to qubit #4 being in the state 1 in the plane spanned by qubit #1 and #2. In the end, qubit #4 will be found in the state 1 if a phase flip has occurred while qubit #3 will be found in the state 1 when a bit flip has occurred. In this case of a Hadamard error, the error detection algorithm will always find that there was some error, as qubit #3 and #4 are anti-correlated as can be seen in DCN.

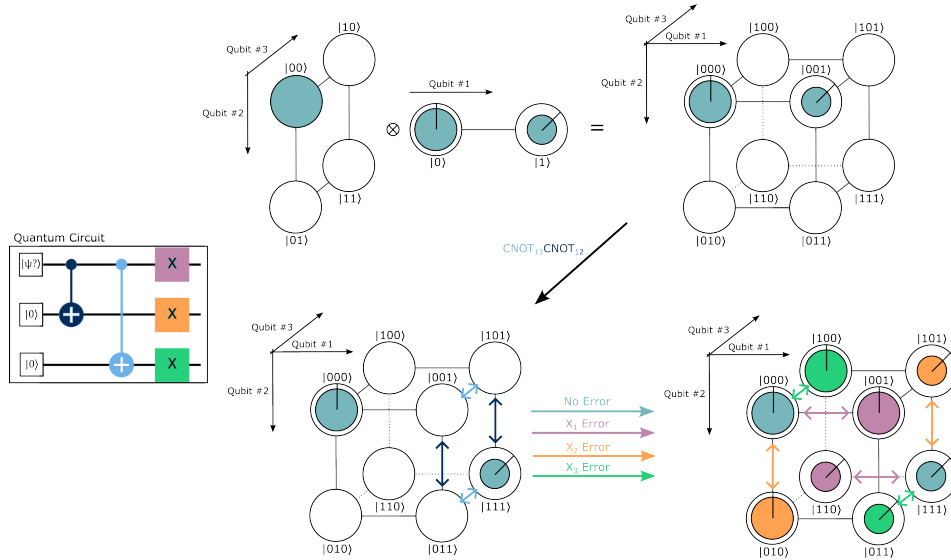


FIG. 17. The initial step of error correcting the (arbitrary) state $|\psi\rangle_1 = \sqrt{2}/\sqrt{3}|0\rangle + 1/\sqrt{3}e^{-i\pi/4}|1\rangle$ using four additional qubits. First, qubit #1 is entangled with qubit #2 and #3 in a GHZ-similar state $|\psi\rangle = \sqrt{2}/\sqrt{3}|000\rangle + 1/\sqrt{3}e^{-i\pi/4}|111\rangle$ with two CNOT gates. Then, a bit flip error is applied. Here, three possible bit flip errors are shown (lilac = bit flip error on qubit #1, orange = bit flip error on qubit #2 and green = bit flip error on qubit #3) as well as the case of no bit flip errors in gray blue. We assume that only one bit flip error occurs at the same time.

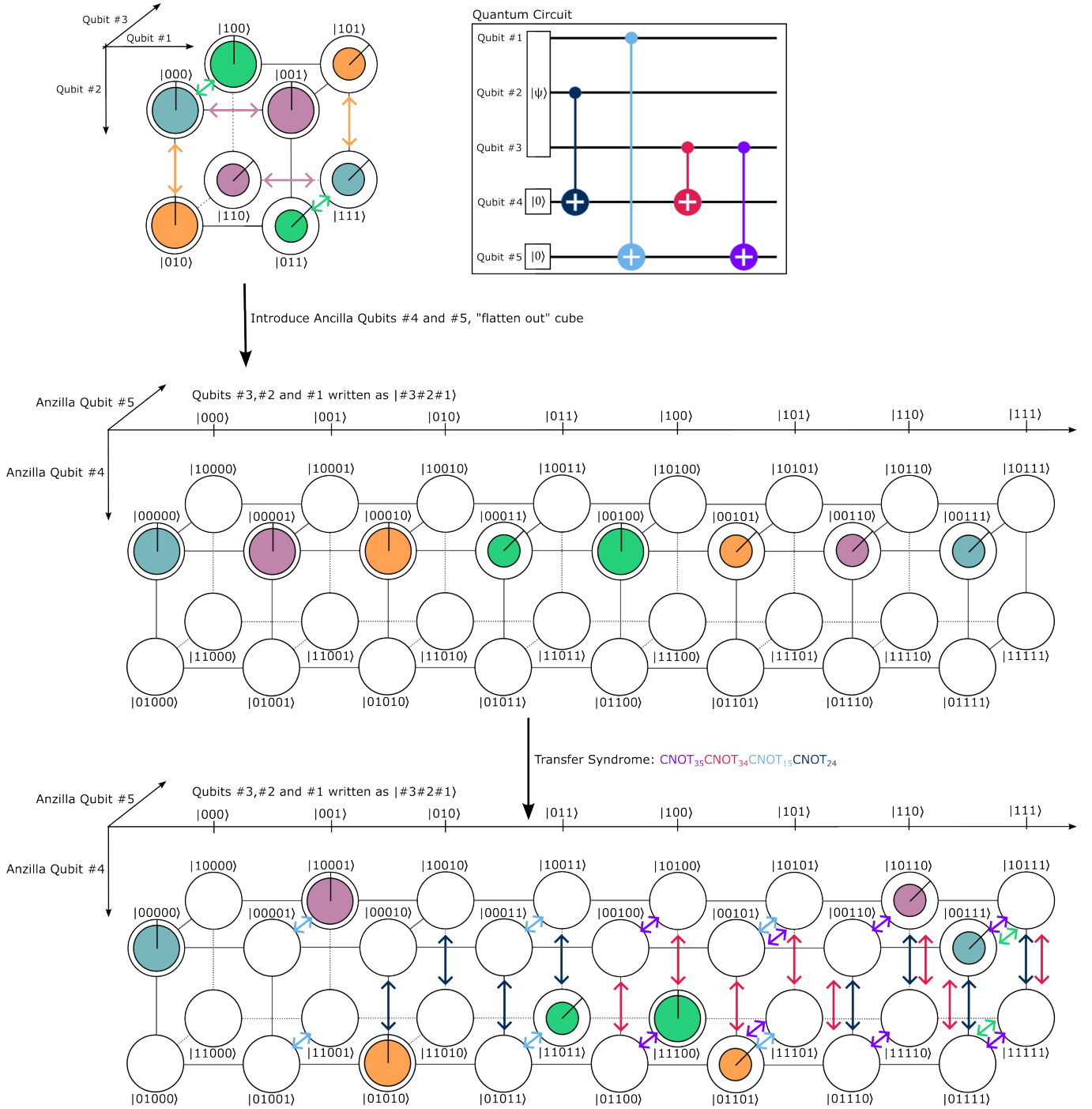


FIG. 18. The "transfer syndrome" step of error correcting the state $|\psi\rangle_1 = \sqrt{2}/\sqrt{3}|0\rangle + 1/\sqrt{3}e^{-i\pi/4}|1\rangle$ using four additional qubits. We start in the final state $|\psi\rangle$ of Fig. 17, flatten out the cube to standard circle notation and introduce the ancilla qubits #4 and #5, arranging the system in modular DCN. The $CNOT_{24}$ - and $CNOT_{34}$ -gates encode an X_2 -error onto ancilla qubit #4 and the $CNOT_{35}$ - and $CNOT_{15}$ -gates encode an X_1 -error onto ancilla qubit #5 while an interesting and desirable byproduct of these operations is that an X_3 -error is encoded on both ancilla qubits.

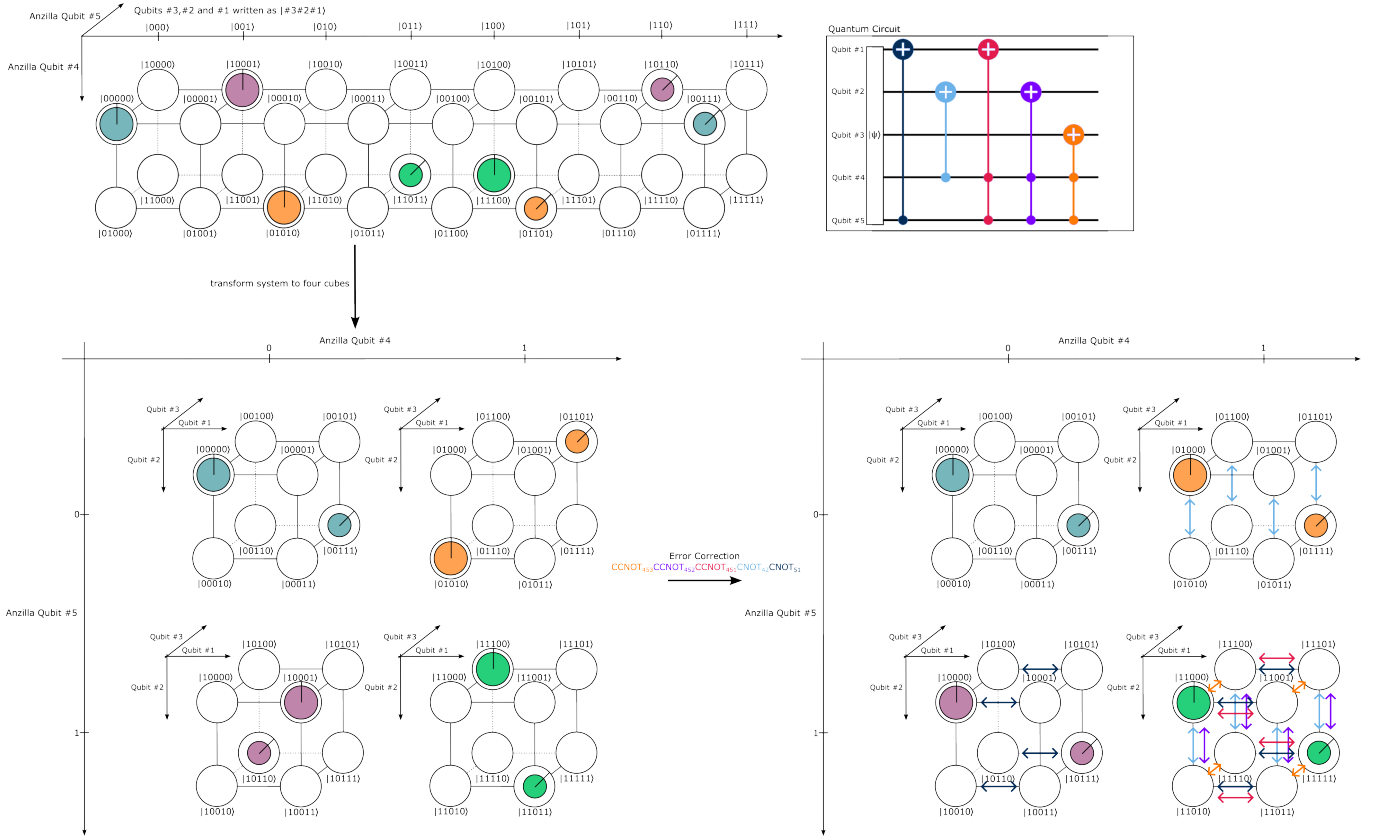


FIG. 19. The last step of error correcting the state $|\psi\rangle_1 = \sqrt{2}/\sqrt{3}|0\rangle + 1/\sqrt{3}e^{-i\pi/4}|1\rangle$. We start by transforming the depiction of the last state $|\psi\rangle$ in Fig. 18 to a four-cube system where the cubes are represented in space depending on ancilla qubit #4 and #5. Here, we can see that the three different kinds of bit flip errors correspond to three different configurations of ancilla qubits #4 and #5. Now, CNOT gates are applied to correct these errors. The CNOT₅₁ gate corrects the X_1 -error, the CNOT₄₂-gate corrects the X_2 -error and the CCNOT₄₅₃-gate corrects the X_3 -error. Lastly, the CCNOT₄₅₂- and CCNOT₄₅₁-gates are needed to counteract the unwanted effects of the first two CNOT-gates in the case of an X_3 -error. Now we can see that in all three cases, qubit #1 is in the desired state $|\psi\rangle_1$. As can be seen, qubit #4 and #5 are now disentangled from the rest of the system and can be measured to see whether a bit flip error has occurred and which one.

Appendix G: Representing partial traces of density matrices of two-qubit systems

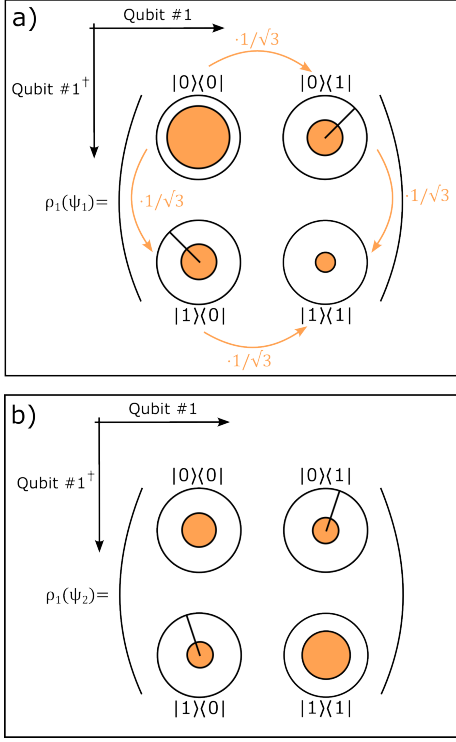


FIG. 20. Partial traces $\rho_1(\psi_1)$ and $\rho_1(\psi_2)$ of the separable state $|\psi_1\rangle = 1/2|00\rangle + 1/\sqrt{12}e^{-i\pi/4}|01\rangle + 1/\sqrt{2}e^{-i\pi/4}|10\rangle + 1/\sqrt{6}e^{-i\pi/2}|11\rangle$ and the entangled state $|\psi_2\rangle = 1/2|00\rangle + 1/\sqrt{12}e^{-i\pi/4}|01\rangle + 1/\sqrt{6}e^{-i\pi/2}|10\rangle + 1/\sqrt{2}e^{-i\pi/4}|11\rangle$. In the case of separability, we find a constant $c = 1/\sqrt{3}e^{-i\pi/4}$. In case of entanglement, we find no such constant.

Density matrices are used to describe general quantum states, including mixed states, and can be used to calculate probabilities of measurement outcomes of observables using the Born rule [55]. Being introduced to the density matrix formalism can come with challenges due to the outer product formulation and to their general abstractness. A general introduction to this formalism can be found in e.g. [56] that visualization could ease the entry to.

In the following we provide a way of representing density matrices of single qubits in DCN and show that the ratio characterization of separability can be seen, i.e. whether the single-qubit state is pure or mixed/part of a larger entangled state. This representation could be incorporated in the DCN web tool, allowing the ability to visually trace out single qubits from the system.

For a general two-qubit state

$$|\psi\rangle = \alpha_{00}|00\rangle + \alpha_{01}|01\rangle + \alpha_{10}|10\rangle + \alpha_{11}|11\rangle \in \mathcal{H}_2 \otimes \mathcal{H}_1 \quad (\text{G1})$$

we can write the density matrix in the computational basis as

$$\rho = |\psi\rangle\langle\psi| = \begin{pmatrix} |\alpha_{00}|^2 & \alpha_{00}\alpha_{01}^* & \alpha_{00}\alpha_{10}^* & \alpha_{00}\alpha_{11}^* \\ \alpha_{01}\alpha_{00}^* & |\alpha_{01}|^2 & \alpha_{01}\alpha_{10}^* & \alpha_{01}\alpha_{11}^* \\ \alpha_{10}\alpha_{00}^* & \alpha_{10}\alpha_{01}^* & |\alpha_{10}|^2 & \alpha_{10}\alpha_{11}^* \\ \alpha_{11}\alpha_{00}^* & \alpha_{11}\alpha_{01}^* & \alpha_{11}\alpha_{10}^* & |\alpha_{11}|^2 \end{pmatrix}, \quad (\text{G2})$$

and tracing out qubit #1 to find the density matrix of qubit #2, we find

$$\rho_2 = \text{tr}_1(\rho) = \begin{pmatrix} |\alpha_{00}|^2 + |\alpha_{01}|^2 & \alpha_{00}\alpha_{10}^* + \alpha_{01}\alpha_{11}^* \\ \alpha_{10}\alpha_{00}^* + \alpha_{11}\alpha_{01}^* & |\alpha_{10}|^2 + |\alpha_{11}|^2 \end{pmatrix}, \quad (\text{G3})$$

whereas

$$\rho_1 = \text{tr}_2(\rho) = \begin{pmatrix} |\alpha_{00}|^2 + |\alpha_{10}|^2 & \alpha_{00}\alpha_{01}^* + \alpha_{10}\alpha_{11}^* \\ \alpha_{01}\alpha_{00}^* + \alpha_{11}\alpha_{10}^* & |\alpha_{01}|^2 + |\alpha_{11}|^2 \end{pmatrix}. \quad (\text{G4})$$

As stated in Sec. IV, one possible characterization of separability is the following: $|\psi\rangle$ is separable if and only if

- i) $\alpha_{00} = \alpha_{10} = 0$ or
- ii) there exists a ratio $c \in \mathbb{C}$ such that $\alpha_{01} = c\alpha_{00}$ and $\alpha_{11} = c\alpha_{10}$.

In the case of i),

$$\rho_1 = \begin{pmatrix} 0 & 0 \\ 0 & 1 \end{pmatrix}. \quad (\text{G5})$$

In the case of ii),

$$\begin{aligned} \rho_1 &= \begin{pmatrix} |\alpha_{00}|^2 + |\alpha_{10}|^2 & c^*(|\alpha_{00}|^2 + |\alpha_{10}|^2) \\ c(|\alpha_{00}|^2 + |\alpha_{10}|^2) & |c|^2(|\alpha_{00}|^2 + |\alpha_{10}|^2) \end{pmatrix} \\ &= \begin{pmatrix} p_1(0) & c^*p_1(0) \\ cp_1(0) & |c|^2p_1(0) \end{pmatrix}. \end{aligned} \quad (\text{G6})$$

where $p_1(0)$ is the probability of obtaining 0 when measuring qubit #1. This way, the ratio characterization of separability can be visually represented as can be seen in Fig. 20. When tracing out qubit #1 to find ρ_2 , we find an analogous and equivalent characterization of separability:

- i) $\alpha_{01} = \alpha_{11} = 0$ or
- ii) there exists a ratio $c' \in \mathbb{C}$ such that $\alpha_{00} = c'\alpha_{01}$ and $\alpha_{10} = c'\alpha_{11}$.

Then we find analogously to above in the case of i)

$$\rho_2 = \begin{pmatrix} 0 & 0 \\ 0 & 1 \end{pmatrix} \quad (\text{G7})$$

and otherwise

$$\rho_2 = \begin{pmatrix} p_2(0) & c'p_2(0) \\ c'^*p_2(0) & |c'|^2p_2(0) \end{pmatrix}. \quad (\text{G8})$$

- [1] D. C. Brody and L. P. Hughston, Geometric quantum mechanics, *Journal of Geometry and Physics* **38**, 19 (2001).
- [2] I. Bengtsson and K. Życzkowski, *Geometry of Quantum States: An Introduction to Quantum Entanglement* (Cambridge University Press, 2006).
- [3] H. Mäkelä and A. Messina, N-qubit states as points on the bloch sphere, *Physica Scripta* **2010**, 014054 (2010).
- [4] M. Boyer, R. Liss, and T. Mor, Geometry of entanglement in the bloch sphere, *Phys. Rev. A* **95**, 032308 (2017).
- [5] O. Gamel, Entangled bloch spheres: Bloch matrix and two-qubit state space, *Phys. Rev. A* **93**, 062320 (2016).
- [6] A. Garon, R. Zeier, and S. J. Glaser, Visualizing operators of coupled spin systems, *Phys. Rev. A* **91**, 042122 (2015).
- [7] S. Heusler, P. Schlummer, and M. S. Ubben, The topological origin of quantum randomness, *Symmetry* **13**, 10.3390/sym13040581 (2021).
- [8] C. Gidney, Visualizing 2-qubit entanglement (2017).
- [9] D. J. Wootton, Visualizing bits and qubits, <https://medium.com/qiskit/visualizing-bits-and-qubits-9af287047b28> (accessed 01-26-2023) (2018).
- [10] The quantum computer puzzle game that matches you against the universe. be a quantum mechanic. (2018).
- [11] M. Ashoori and J. D. Weisz, Entanglion (2018).
- [12] Hello quantum: The making of a seriously fun quantum game (2019).
- [13] M. Backens, The ZX-calculus is complete for stabilizer quantum mechanics, *New Journal of Physics* **16**, 093021 (2014).
- [14] A. Hadzihasanovic, A diagrammatic axiomatisation for qubit entanglement, in *2015 30th Annual ACM/IEEE Symposium on Logic in Computer Science* (2015) pp. 573–584.
- [15] K. F. Ng and Q. Wang, A universal completion of the zx-calculus (2017), arXiv:1706.09877 [quant-ph].
- [16] M. Backens and A. Kissinger, ZH: A complete graphical calculus for quantum computations involving classical non-linearity, *Electronic Proceedings in Theoretical Computer Science* **287**, 23 (2019).
- [17] E. R. Johnston, N. Harrigan, and M. Gimeno-Segovia, *Programming Quantum Computers: Essential algorithms and code samples* (O’Reilly Media, Incorporated, 2019).
- [18] B. Just, *Quantencomputing Kompakt: Spukhafte Fernwirkung und teleportation endlich verständlich* (Springer Vieweg, 2020).
- [19] S. Ainsworth, Deft: A conceptual framework for considering learning with multiple representations, *Learning and Instruction* **16**, 183 (2006).
- [20] L. Hu, G. Chen, P. Li, and J. Huang, Multimedia effect in problem solving: A meta-analysis, *Educational Psychology Review* **33**, 1717 (2021).
- [21] A. V. Thapliyal, Multipartite pure-state entanglement, *Phys. Rev. A* **59**, 3336 (1999).
- [22] W. Dür and J. I. Cirac, Multiparticle entanglement and its experimental detection, *Journal of Physics A: Mathematical and General* **34**, 6837 (2001).
- [23] G. Brassard and T. Mor, Multi-particle entanglement via two-party entanglement, *Journal of Physics A: Mathematical and General* **34**, 6807 (2001).
- [24] C.-S. Yu and H.-S. Song, Full separability criterion for tripartite quantum systems, *The European Physical Journal D* **42**, 147 (2007).
- [25] M. Seevinck and J. Uffink, Partial separability and entanglement criteria for multiqubit quantum states, *Phys. Rev. A* **78**, 032101 (2008).
- [26] O. Gühne and M. Seevinck, Separability criteria for genuine multiparticle entanglement, *New Journal of Physics* **12**, 053002 (2010).
- [27] J.-L. Li and C.-F. Qiao, A necessary and sufficient criterion for the separability of quantum state, *Scientific Reports* **8**, 1442 (2018).
- [28] R. E. Mayer, Cognitive theory of multimedia learning, *The Cambridge handbook of multimedia learning* **49** (2005).
- [29] W. Schnotz, An integrated model of text and picture comprehension, *The Cambridge handbook of multimedia learning* **49** (2005).
- [30] T. Fredlund, C. Linder, J. Airey, and A. Linder, Unpacking physics representations: Towards an appreciation of disciplinary affordance, *Physical Review Special Topics-Physics Education Research* **10**, 020129 (2014).
- [31] M. A. Rau, Conditions for the effectiveness of multiple visual representations in enhancing stem learning, *Educational Psychology Review* **29**, 717 (2017).
- [32] J. L. Cooper, P. G. Sidney, and M. W. Alibali, Who benefits from diagrams and illustrations in math problems? ability and attitudes matter, *Applied Cognitive Psychology* **32**, 24 (2018).
- [33] W. K. Wootters, Entanglement of formation and concurrence., *Quantum Inf. Comput.* **1**, 27 (2001).
- [34] A. Peres and D. R. Terno, Quantum information and relativity theory, *Reviews of Modern Physics* **76**, 93 (2004).
- [35] L. B. Kish, ‘quantum supremacy’ revisited: low-complexity, deterministic solutions of the original deutsch–jozsa problem in classical physical systems, *Royal Society Open Science* **10**, 221327 (2023), <https://royalsocietypublishing.org/doi/pdf/10.1098/rsos.221327>.
- [36] P. JORRAND and M. MHALLA, Separability of pure n-qubit states: Two characterizations, *International Journal of Foundations of Computer Science* **14**, 797 (2003), <https://doi.org/10.1142/S0129054103002035>.
- [37] H. Matsueda and D. Cohen, Dynamic entanglement and separability criteria for quantum computing bit states, *International Journal of Theoretical Physics* **46**, 3169 (2007).
- [38] N. Gisin and R. Thew, Quantum communication, *Nature Photonics* **1**, 165 (2007).
- [39] S. Hillmich, A. Zulehner, and R. Wille, Exploiting quantum teleportation in quantum circuit mapping, in *Proceedings of the 26th Asia and South Pacific Design Automation Conference, ASPDAC ’21* (Association for Computing Machinery, New York, NY, USA, 2021) p. 792–797.
- [40] M.-C. Chen, R. Li, L. Gan, X. Zhu, G. Yang, C.-Y. Lu, and J.-W. Pan, Quantum-teleportation-inspired algorithm for sampling large random quantum circuits, *Phys. Rev. Lett.* **124**, 080502 (2020).
- [41] S. Pirandola, J. Eisert, C. Weedbrook, A. Furusawa, and S. L. Braunstein, Advances in quantum teleportation,

- Nature Photonics **9**, 641 (2015).
- [42] J. C. Meyer, G. Passante, S. J. Pollock, and B. R. Wilcox, Today's interdisciplinary quantum information classroom: Themes from a survey of quantum information science instructors, *Phys. Rev. Phys. Educ. Res.* **18**, 010150 (2022).
- [43] Y. Wang, Z. Hu, B. C. Sanders, and S. Kais, Qudits and high-dimensional quantum computing, *Frontiers in Physics* **8**, 10.3389/fphy.2020.589504 (2020).
- [44] Y. Chi, J. Huang, Z. Zhang, J. Mao, Z. Zhou, X. Chen, C. Zhai, J. Bao, T. Dai, H. Yuan, M. Zhang, D. Dai, B. Tang, Y. Yang, Z. Li, Y. Ding, L. K. Oxenløwe, M. G. Thompson, J. L. O'Brien, Y. Li, Q. Gong, and J. Wang, A programmable qudit-based quantum processor, *Nature Communications* **13**, 1166 (2022).
- [45] T. Roy, Z. Li, E. Kapit, and D. I. Schuster, Realization of two-qutrit quantum algorithms on a programmable superconducting processor (2022), arXiv:2211.06523 [quant-ph].
- [46] C. M. Lee and J. H. Selby, Generalised phase kick-back: the structure of computational algorithms from physical principles, *New Journal of Physics* **18**, 033023 (2016).
- [47] B. A. Bellcore, B. Aiello, Bellcore, T. L. M. Department, L. for Computer Science, T. Leighton, M. Department, L. for Computer Science, M. I. o. Technology, and O. M. A. Metrics, Coding theory, hypercube embeddings, and fault tolerance: Proceedings of the third annual acm symposium on parallel algorithms and architectures (1991).
- [48] O. Frieder, F. Harary, and P.-J. Wan, A radio coloring of a hypercube, *International Journal of Computer Mathematics* **79**, 665 (2002), <https://doi.org/10.1080/00207160211287>.
- [49] W. Aiello and F. T. Leighton, Hamming codes, hypercube embeddings, and fault tolerance, *SIAM Journal on Computing* **37**, 783 (2007), <https://doi.org/10.1137/S0097539798332464>.
- [50] A. Kubica, B. Yoshida, and F. Pastawski, Unfolding the color code, *New Journal of Physics* **17**, 083026 (2015).
- [51] M. Vasmer and A. Kubica, Morphing quantum codes, *PRX Quantum* **3**, 10.1103/prxquantum.3.030319 (2022).
- [52] A. D. Córcoles, E. Magesan, S. J. Srinivasan, A. W. Cross, M. Steffen, J. M. Gambetta, and J. M. Chow, Demonstration of a quantum error detection code using a square lattice of four superconducting qubits, *Nature Communications* **6**, 6979 (2015).
- [53] M. Gong, X. Yuan, S. Wang, Y. Wu, Y. Zhao, C. Zha, S. Li, Z. Zhang, Q. Zhao, Y. Liu, F. Liang, J. Lin, Y. Xu, H. Deng, H. Rong, H. Lu, S. C. Benjamin, C.-Z. Peng, X. Ma, Y.-A. Chen, X. Zhu, and J.-W. Pan, Experimental exploration of five-qubit quantum error-correcting code with superconducting qubits, *National Science Review* **9**, 10.1093/nsr/nwab011 (2021), nwab011, https://academic.oup.com/nsr/article-pdf/9/1/nwab011/44252340/nwab011_supplemental_file.pdf.
- [54] V. KASIRAJAN, *Fundamentals of quantum computing: Theory and practice* (SPRINGER, 2022).
- [55] N. P. Landsman, Born rule and its interpretation, in *Compendium of Quantum Physics*, edited by D. Greenberger, K. Hentschel, and F. Weinert (Springer Berlin Heidelberg, Berlin, Heidelberg, 2009) pp. 64–70.
- [56] M. A. Nielsen and I. L. Chuang, *Quantum Computation and Quantum Information: 10th Anniversary Edition* (Cambridge University Press, 2011).